Title

Structural diversity in Ni II cluster chemistry: Ni 5 , Ni 6 , and {NiNa 2 } n complexes bearing the Schiff-base ligand N -naphthalidene-2-amino-5-chlorobenzoic acid

Journal

Dalton Transactions, 45(25)

ISSN

1477-9226

Authors

Perlepe, Panagiota S

Cunha-Silva, Luís

Bekiari, Vlasoula

et al.

Publication Date

2016-06-21

DOI

10.1039/c6dt01162d

Peer reviewed

Structural diversity in Ni^{II} cluster chemistry: Ni_5, Ni_6, and $\{NiNa_2\}_n$ complexes bearing the Schiff-base ligand *N*-naphthalidene-2-amino-5-chlorobenzoic acid†

Panagiota S. Perlepe,[a] Luís Cunha-Silva,[b] Vlasoula Bekiari,[c] Kevin J. Gagnon,[d] Simon J. Teat,[d] Albert Escuer[e] and Theocharis C. Stamatatos*[a]

The employment of the fluorescent bridging and chelating ligand *N*-naphthalidene-2-amino-5-chlorobenzoic acid ($nacbH_2$) in Ni^{II} cluster chemistry has led to a series of pentanuclear and hexanuclear compounds with different structural motifs, magnetic and optical properties, as well as an interesting 1-D coordination polymer. Synthetic parameters such as the inorganic anion present in the NiX_2 starting materials (X = ClO_4^- or Cl^-), the reaction solvent and the nature of the organic base employed for the deprotonation of $nacbH_2$ were proved to be structure-directing components. Undoubtedly, the reported results demonstrate the rich coordination chemistry of $nacbH_2$ in the presence of Ni^{II} metal ions and the ability of this chelate to adopt a variety of different modes, thus fostering the formation of high-nuclearity molecules with many physical properties.

Introduction

The quest for high-nuclearity metal complexes of paramagnetic 3d-metal ions has intensified over the last decade or so due to their inherent architectural beauty[1] and interesting properties, such as magnetic,[2] optical,[3] catalytic,[4] and biological.[5] The synthesis of such 0-D molecular compounds is largely based on serendipity (or 'self-assembly') but such a lack of design and prediction does actually bring into the field all the intriguing and special structural and physicochemical features that these molecules exhibit.[6] The success of this approach mainly stems from the choice of the primary organic chelating/bridging ligand and afterwards from the systematic investigation of the effect of all possible synthetic variables on the chemical and structural identities of the resulting species. For a given organic chelate, some of the synthetic variables that worth exploration are the type of metal salts used as precursors, the metal-to-ligand ratio, the reaction solvent, the temperature and the crystallization methods.[7]

Polynuclear Ni^{II} complexes have shown some promise as high-spin molecules and candidates for single-molecule magnetism behaviors.[8] In 3d-metal cluster chemistry, high-spin molecules with large ground state spin values, *S*, result ideally from ferromagnetic exchange interactions between the paramagnetic metal ions or from the presence of spin frustration effects on antiferromagnetically-coupled systems. Spin frustration can be defined in its general sense as the occurrence of competing exchange interactions of comparable magnitude that prevent (frustrate) the preferred spin alignments. For example, in certain topologies, such as metal triangles, the spins of two antiferromagnetically-coupled metal ions (or other spin carriers) may be forced into a parallel alignment by other, stronger interactions; thus, the intrinsic preference of the spins to align antiparallel is frustrated.[9] When a system with an appreciable *S* value is further combined with a significant magnetic anisotropy of an Ising (or easy-axis) type, then an energy barrier to magnetization reversal is generated and the compound can behave as single-molecule magnet (SMM).[10] SMMs represent a molecular or "bottom-up" approach to nanoscale magnetism with potential applications in the fields of information storage, molecular electronics and spintronics.[11]

Organic and inorganic bridging ligands of various types have been utilized over the last three decades for the synthesis of both high-spin clusters and SMMs.[6,12] However, the investigation of the optical properties of these superparamagnetic-like 3d-metal species has been always deterrent, probably due to problems arising from quenching effects from both the paramagnetic metals and the coordinated ligands and solvate molecules.[13] We have thus decided to start working with a ligand that could in principle tackle all of these obstacles and contribute towards the synthesis of new polynuclear Ni^{II} clusters with unprecedented structures and both interesting magnetic and optical properties. The ligand of choice in this study was the tetradentate Schiff base *N*-naphthalidene-2-amino-5-chlorobenzoic acid ($nacbH_2$, Scheme 1). $NacbH_2$ is a fluorescent ligand and has limited previous use in 3d-metal cluster chemistry, from which we have been able to isolate and characterize a Ni_{12} wheel-like cluster and a Ni_5 zigzag

[a] *Department of Chemistry, Brock University, St. Catharines, Ontario L2S 3A1, Canada*
[b] *REQUIMTE / LAQV & Department of Chemistry and Biochemistry, Faculty of Sciences, University of Porto, 4169-007 Porto, Portugal*
[c] *Department of Aquaculture and Fisheries Management, Technological Educational Institute of Western Greece, 30 200 Messolonghi, Greece*
[d] *Advanced Light Source, Lawrence Berkeley National Laboratory, 1 Cyclotron Road, Berkeley, CA 94720, USA*
[e] *Departament de Quimica Inorganica and Institut de Nanociencia i Nanotecnologia (IN²UB), Universitat de Barcelona, Diagonal 645, 08028 Barcelona, Spain*

† Electronic Supplementary Information (ESI) available: Crystallographic data of complexes **1**-**6** in CIF formats. See DOI: 10.1039/x0xx00000x

compound exhibiting a unique ligand transformation to a hydroquinone-functionalized Schiff base.[14]

We here report our results from the systematic study of the coordination and bridging affinity of $nacbH_2$ in Ni^{II} chemistry in the absence of any additional bridging groups such as pseudohalides and/or carboxylates. We also show that the inorganic anions present in the Ni^{II} starting materials (ClO_4^- vs. Cl^-), the nature of the reaction solvent(s), and the type of base used (organic vs. inorganic) have drastically affected the chemical and structural identities of the resulting compounds. Hence, three Ni_5 and two Ni_6 clusters with different topologies, as well as a 1-D coordination polymer consisting of $NiNa_2$ repeating units, were synthesized and characterized in terms of their magnetic and emissive responses.

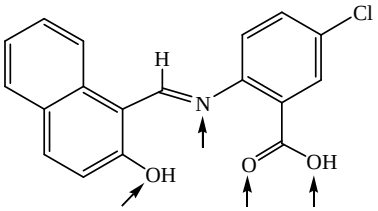

N-naphthalidene-2-amino-5-chlorobenzoic acid

nacbH$_2$

Scheme 1 Structural formula and abbreviation of the organic chelating/bridging ligand used in this work. The arrows indicate the potential donor atoms.

Experimental Section

Syntheses

All manipulations were performed under aerobic conditions using chemicals and solvents as received. The ligand $nacbH_2$ was synthesized and adequately characterized (^1H and ^{13}C NMR, IR and elemental analyses) as previously reported.[14] Safety note: Perchlorate salts are potentially explosive; such compounds should be synthesized and used in small quantities, and treated with utmost care at all times.

[Ni$_5$(OMe)$_2$(nacb)$_4$(MeOH)$_3$] (1). To a stirred, orange suspension of $nacbH_2$ (0.07 g, 0.2 mmol) in MeOH (15 mL) was added NEt_3 (56 µL, 0.4 mmol). The resulting yellow solution was stirred for 5 min, during which time solid $Ni(ClO_4)_2{\cdot}6H_2O$ (0.07 g, 0.2 mmol) was added and the color of the solution changed to dark orange-brown. Additional stirring for 15 min did not alter the color or form of the solution. The latter was then filtered, and the filtrate was diffused with hexanes (10 mL) and left undisturbed at ambient temperature to afford after ~12 days green-yellow crystals of **1**•5MeOH•2(C_6H_{14}). The crystals were collected by filtration, washed with cold MeOH (2 x 2 mL) and dried in air. The yield was 52%. Elemental analysis (%) calcd for the lattice solvent-free **1**: C 52.67, H 3.51, N 3.15; found: C 52.79, H 3.65, N 3.09. Selected IR data (ATR): *v* = 1579 (s), 1534 (vs), 1451 (s), 1425 (m), 1395 (s), 1350 (s), 1300 (m), 1249 (s), 1181 (m), 1159 (m), 1114 (m), 1091 (m), 1029 (w), 992 (m), 960 (m), 887 (m), 852 (m), 816 (vs), 774 (m), 742 (vs), 635 (m), 563 (m), 510 (m), 421 (m).

[Ni$_5$(OH)$_2$(nacb)$_4$(DMF)$_4$] (2). This complex was prepared in the exact same manner as complex **1**, but using DMF (15 mL) in place of MeOH. After 20 days, X-ray quality green-yellow crystals of **2**•3DMF were collected by filtration, washed with cold DMF (2 x 2 mL) and dried under vacuum. The yield was 40%. Elemental analysis (%) calcd for **2**: C 52.69, H 3.68, N 5.85; found: C 52.84, H 3.91, N 5.66. Selected IR data (ATR): *v* = 2923 (w), 1659 (s), 1581 (s), 1532 (vs), 1451 (vs), 1380 (s), 1352 (s), 1251 (s), 1178 (m), 1090 (m), 962 (m), 826 (vs), 745 (vs), 636 (m), 564 (m), 506 (m), 418 (m).

[Ni$_5$(OMe)Cl(nacb)$_4$(MeOH)$_3$(MeCN)] (3). To a stirred, orange suspension of $nacbH_2$ (0.07 g, 0.2 mmol) in MeCN/MeOH (15 mL, 2:1 v/v) was added NEt_3 (56 µL, 0.4 mmol). The resulting yellow solution was stirred for 5 min, during which time solid $NiCl_2{\cdot}6H_2O$ (0.10 g, 0.4 mmol) was added and the color of the solution changed to orange-brown. Additional stirring for 15 min did not alter the color and form of the solution. The latter was then filtered, and the filtrate was diffused into a mixture of Et_2O/hexanes (30 mL, 1:1 v/v) to afford after 2 days olive-green crystals of **3**·4MeCN·4MeOH·Et_2O. The crystals were collected by filtration, washed with cold MeOH (2 x 2 mL) and Et_2O (2 x 2 mL) and dried under vacuum. The yield was 43%. Elemental analysis (%) calcd for **3**•MeCN: C 52.42, H 3.35, N 4.58; found: C 52.33, H 3.23, N 4.76. Selected IR data (ATR): *v* = 2950 (s), 1582 (m), 1535 (s), 1453 (s), 1428 (s), 1388 (vs), 1364 (vs), 1228 (s), 1182 (s), 1159 (s), 1116 (m), 1039 (w), 984 (m), 961 (m), 900 (w), 830 (m), 779 (m), 747 (s), 664 (w), 637 (m), 550 (w), 509 (w), 456 (m).

(NHEt$_3$)$_2$[Ni$_6$(OH)$_2$(nacb)$_6$(H$_2$O)$_4$] (4). To a stirred, orange suspension of $nacbH_2$ (0.07 g, 0.2 mmol) in CH_2Cl_2 (20 mL) was added NEt_3 (56 µL, 0.4 mmol). The resulting yellow solution was stirred for 5 min, during which time solid $NiCl_2{\cdot}6H_2O$ (0.10 g, 0.4 mmol) was added and the color of the solution turned orange. Additional stirring for 30 min did not alter further the color and form of the solution. The latter was then filtered, and the filtrate was left undisturbed at room temperature to slowly evaporate and afford after 18 days, X-ray quality orange crystals of **4**·8CH_2Cl_2. The crystals were collected by filtration, washed with cold CH_2Cl_2 (2 × 2 mL) and dried under vacuum. The yield was 63%. Elemental analysis (%) calcd for the lattice solvent-free **4**: C 55.33, H 3.95, N 4.30; found: C 55.38, H 4.11, N 4.15. Selected IR data (ATR): *v* = 3042 (wb), 1579 (vs), 1555 (m), 1534 (s), 1450 (s), 1428 (s), 1388 (m), 1340 (m), 1253 (m), 1179 (s), 1155 (s), 1112 (m), 1089 (m), 984 (s), 960 (m), 884 (m), 853 (w), 820 (s), 777 (m), 740 (vs), 634 (m), 553 (m), 504 (m), 458(m).

{[NiNa$_2$(nacb)$_2$(MeOH)$_2$]·[NiNa$_2$(nacb)$_2$(MeOH)$_2$(H$_2$O)$_2$]}$_n$ (5). To a stirred, orange suspension of $nacbH_2$ (0.07 g, 0.2 mmol) in CH_2Cl_2/MeOH (25 mL, 4:1 v/v) was added solid NaOH (0.02 g, 0.4 mmol). The resulting orange suspension was stirred for 10 min, during which time solid $NiCl_2{\cdot}6H_2O$ (0.10 g, 0.4 mmol) was added and the color of the solution

turned olive-green. Additional stirring for an hour led to a brownish suspension which was filtered, and the filtrate was left undisturbed to slowly evaporate at room temperature. After ~25 days, X-ray quality crystals of **5** were precipitated and collected by filtration. The crystals were washed with cold MeOH (2 x 2 mL) and dried in air. The yield was 32%. Elemental analysis (%) calcd for **5**: C 54.71, H 3.62, N 3.36; found: C 54.51, H 3.43, N 3.49. Selected IR data (ATR): *v* = 3044 (wb), 1576 (vs), 1534 (vs), 1492 (vs), 1448 (s), 1428 (m), 1381 (m), 1352 (m), 1252 (s), 1176 (vs), 1152 (m), 1034 (m), 991 (m), 889 (s), 816 (s), 768 (m), 739 (m), 614 (m), 517 (m), 457 (m).

$[Ni_6(nacb)_6(H_2O)_3(MeOH)_6]$ (6). To a stirred, orange suspension of $nacbH_2$ (0.07 g, 0.2 mmol) in CH_2Cl_2/MeOH (25 mL, 4:1 v/v) was added solid KOH (0.02 g, 0.4 mmol). The resulting orange suspension was stirred for 10 min, during which time solid $NiCl_2{\cdot}6H_2O$ (0.10 g, 0.4 mmol) was added and the color of the solution turned light-brown. Additional stirring for an hour led to a brownish suspension which was filtered, and the filtrate was left undisturbed to slowly evaporate at room temperature. After ~30 days, X-ray quality crystals of **6**$\bullet 2CH_2Cl_2\bullet H_2O$ were precipitated and collected by filtration. The crystals were washed with cold MeOH (2 x 2 mL) and dried in air. The yield was 20%. Elemental analysis (%) calcd for **6**$\bullet H_2O$: C 53.51, H 3.62, N 3.28; found: C 53.66, H 3.81, N 3.20. Selected IR data (ATR): *v* = 3587 (w), 2917 (wb), 1615 (m), 1576 (vs), 1533 (vs), 1450 (vs), 1426 (m), 1385 (m), 1340 (m), 1251 (s), 1178 (vs), 1156 (m), 1113 (m), 1090 (m), 982 (m), 889 (s), 819 (vs), 776 (w), 740 (vs), 661 (m), 559 (w), 509 (m), 455 (m).

X-ray Crystallography

Crystalline materials of complexes **1**-**5** were manually harvested, and selected single-crystals of each compound were mounted on cryoloops using adequate oil.[15] Diffraction data were collected at 150(2) K on a Bruker X8 Kappa APEX II Charge-Coupled Device (CCD) area-detector diffractometer controlled by the APEX2 software package (MoKα graphite-monochromated radiation, λ = 0.71073 Å),[16] and equipped with an Oxford Cryosystems Series 700 cryostream monitored remotely with the software interface Cryopad.[17] Data for complex **6** were collected on beamline 11.3.1 at the Advanced Light Source, Lawrence Berkeley National Lab. Samples were mounted on MiTeGen® kapton loops and placed in a 100(2) K nitrogen cold stream provided by an Oxford Cryostream 700 Plus low temperature apparatus on the goniometer head of a Bruker D8 diffractometer equipped with a PHOTON100 CMOS detector operating in shutterless mode. Diffraction data were collected using synchrotron radiation monochromated using silicon(111) to a wavelength of 0.7749(1) Å. An approximate full-sphere of data was collected using a combination of phi and omega scans with scan speeds of 1 second per 4 degrees for the phi scans, and 5 seconds per degree for the omega scans at 2θ = 0 and -45, respectively.

The images obtained during the data collection for all complexes **1**-**6** were processed with the software SAINT+,[18] and the absorption effects were corrected by the multi-scan method implemented in SADABS.[19] The structures were solved using the algorithm implemented in SHELXT,[20,21] and refined by successive full-matrix least-squares cycles on F^2 using the latest SHELXL-v.2014.[20,22] All the non-hydrogen atoms were successfully refined using anisotropic displacement parameters. Hydrogen atoms on aliphatic and aromatic carbon atoms were geometrically located using appropriate *HFIX* instructions in SHELXL, and included in subsequent refinement cycles in riding-motion approximation with isotropic thermal displacement parameters (U_{iso}) fixed at 1.2 or 1.5 × U_{eq} of the relative atom. Most of the hydrogen atoms on the bound methanol and water molecules were found in the Fourier difference maps, their distances were fixed and allowed to refine with a riding model. The structures of complexes **1**-**4** and **6** contain solvent channels which could not be modeled and were treated with the program SQUEEZE,[23] as implemented in the software package PLATON.[24] In one of the two coordination polymers that crystallize in **5** (the one containing Ni2) the two Na^+ cations are disordered over 4 positions, as well as the two coordinated water molecules which are also disordered over 4 possible positions.

Additional information about crystallographic data collection and structure refinement details are summarized in Table 1. Crystallographic data for the reported structures have been deposited with the Cambridge Crystallographic Data Centre (CCDC) as supplementary publication numbers: CCDC-1448720 to 1448725 for complexes **1** to **6**, respectively. Copies of these data can be obtained free of charge via *https://summary.ccdc.cam.ac.uk/structure-summary-form*.

Physical Measurements

Infrared spectra were recorded in the solid state on a Bruker's FT-IR spectrometer (ALPHA's Platinum ATR single reflection) in the 4000-400 cm^{-1} range. Elemental analyses (C, H, and N) were performed on a Perkin-Elmer 2400 Series II Analyzer. Excitation and emission spectra were recorded in the solid state using a Cary Eclipse spectrofluorometer. Magnetic susceptibility studies were performed at the Chemistry Department of the University of Barcelona on a MPMS5 Quantum Design magnetometer. Pascal's constants were used to estimate the diamagnetic correction, which was subtracted from the experimental susceptibility to give the molar paramagnetic susceptibility (χ_M).[25] The magnetic data of all complexes were fitted to the appropriate spin Hamiltonians (*vide infra*) using the PHI software.[26] The quality of the fits was parameterized as the factor $R = (\chi_M T_{exp}-\chi_M T_{calc})^2/(\chi_M T_{exp})^2$.

Results and Discussion

Synthetic Comments

There are similarities as well as important differences in the synthetic routes followed for the isolation of the reported

compounds. In all the cases, we utilized tertiary reaction systems containing a NiX_2 reagent, the ligand of choice, $nacbH_2$, and a base to abstract the protons of the ligand's OH groups, at different solvents and solvent mixtures. We employed two different NiX_2 starting materials, one containing the poorly coordinated ClO_4^- anion and the other including the Cl^- anion which is known to exhibit a better coordinating affinity for 1st-row transition metal ions. Both ClO_4^- and Cl^- anions are weak Brönsted bases; therefore, the addition of an external base seemed necessary for the facilitation of the ligand's deprotonation. We used three different bases in total which all led us to the isolation of different products (*vide infra*); upon proton abstraction by the organic base NEt_3, the resulting $NHEt_3^+$ species can frequently counterbalance the anionic charge of a cluster compound in solution and consequently help with the crystallization of the resulting salt in the solid-state. In contrast, the strong inorganic bases, such as the NaOH and KOH, can supply the resulting solutions with the corresponding hydrated Na^+ and K^+ cations which are more susceptible in binding with O- and N-donor ligands rather than counterbalancing the charge of an anionic cluster compound.[27] Furthermore, another important synthetic factor that is worthy investigating is the effect of the solvent on the structural identity of cluster compounds. The volatility, polarity, rigidity and coordination affinity of reaction solvents are some of the parameters which could affect the thermodynamics and kinetics of a product's formation in solution, and consequently the chemical identity of a species in the solid-state.[28]

To that end, the initial reaction between $Ni(ClO_4)_2{\cdot}6H_2O$, $nacbH_2$ and NEt_3 in a molar ratio of 1:1:2 in MeOH led to the subsequent formation of complex $[Ni_5(OMe)_2(nacb)_4(MeOH)_3]$ (**1**) in 52% yield. In an attempt to investigate the effect of the reaction solvent on the structural identity of **1**, we performed the exact same reaction but in a variety of polar and non-polar solvent media. Only when the reaction was carried out in DMF we were able to isolate a crystalline compound, and this was identified as complex $[Ni_5(OH)_2(nacb)_4(DMF)_4]$ (**2**) which is structurally similar to **1** (*vide infra*). In our next synthetic efforts, we focused on the use of $NiCl_2{\cdot}6H_2O$ as a metal-containing starting material. From the 2:1:2 reaction between $NiCl_2{\cdot}6H_2O$, $nacbH_2$ and NEt_3 in a solvent mixture comprising MeCN and MeOH, we were able to crystallize and characterize the new pentanuclear compound $[Ni_5(OMe)Cl(nacb)_4(MeOH)_3(MeCN)]$ (**3**) in 43% yield. Since complex **3** contains bound solvate molecules, we decided to change the solvent and perform the same reaction in CH_2Cl_2 which has a negligible binding affinity towards 3d-metal ions in moderate-to-high oxidation states. We were very pleased to see that the crystallized compound was this time a hexanuclear $(NHEt_3)_2[Ni_6(OH)_2(nacb)_6(H_2O)_4]$ (**4**) compound, isolated in 63% yield. The fact that the formula of the anionic compound **4** was counterbalanced by two Et_3NH^+ cations let us think that a change of base from an organic to an inorganic one could lead us to a different complex. Indeed, the same reaction that led to **4**, but with NaOH in place of NEt_3, allowed us to isolate a new coordination polymer $\{[NiNa_2(nacb)_2(MeOH)_2]\bullet[NiNa_2(nacb)_2(MeOH)_2(H_2O)_2]\}_n$ (**5**) in 32% overall yield. The polymeric compound **5** contains both Ni^{II} and Na^{I} coordinated cations (*vide infra*), confirming the coordination affinity of alkali metals towards ligands with N- and O-donor atoms. In the reaction mixture that led to **5**, a second solvent MeOH was also employed in conjunction with CH_2Cl_2 in order to enhance the solubility of the solid NaOH. With complex **5** in hand, we decided to investigate the effect of the alkali metal on the chemical identity of $Ni^{II}/nacb^{2-}$ compounds. The exact same reaction that yielded **5** was repeated with KOH instead of NaOH but the crystallization of the resulting solution afforded this time crystals of a new hexanuclear $[Ni_6(nacb)_6(H_2O)_3(MeOH)_6]$ (**6**) compound in comparable with **5** yields (~20%). A distinct difference between **6** and **5** is the absence of coordinated K^+ cations in the former, which could be only tentatively assigned to the differences in sizes (ionic radii: Na^+, 116 pm; K^+, 152 pm) between the two cations under the same reaction conditions.

Table 1 Crystallographic data for complexes **1**-**6**

Parameter	**1**·5MeOH·2(C_6H_{14})	**2**·3DMF	**3**·4MeCN·4MeOH·Et_2O	**4**·8CH_2Cl_2	**5**	**6**
Formula	$C_{94}H_{106}Cl_4N_4Ni_5O_{22}$	$C_{93}H_{91}Cl_4N_{11}Ni_5O_{21}$	$C_{94}H_{96}Cl_5N_9Ni_5O_{21}$	$C_{128}H_{118}Cl_{22}N_8Ni_6O_{24}$	$C_{76}H_{60}Cl_4N_4Na_4Ni_2O_{18}$	$C_{116}H_{96}Cl_{10}N_6Ni_6O_{27.29}$
Fw / g mol^{-1}	2079.17	2134.11	2158.59	3284.46	1668.46	2717.42
Crystal type	Green plate	Green plate	Green plate	Orange needle	Orange needle	Yellow rod
Crystal size / mm^3	0.10×0.07×0.05	0.30×0.10×0.03	0.31×0.17×0.12	0.35×0.16×0.11	0.37×0.08×0.07	0.11×0.04×0.02
Crystal system	Triclinic	Triclinic	Triclinic	Monoclinic	Triclinic	Orthorhombic
Space group	*P*-1	*P*-1	*P*-1	$P2_1/n$	*P*-1	*Pbca*
a / Å	14.472(2)	14.1417(10)	17.414(4)	14.7531(12)	7.5505(16)	27.5171(11)
b / Å	14.473(2)	14.1587(10)	17.728(4)	18.2554(16)	18.877(4)	27.7084(10)
c / Å	24.048(4)	14.7117(11)	18.040(4)	26.332(2)	26.086(6)	31.0222(12)
α / °	101.736(8)	92.408(2)	69.585(9)	90	79.415(11)	90
β / °	96.477(8)	99.389(2)	84.074(9)	99.008(4)	86.090(10)	90
γ / °	116.529(7)	116.998(2)	65.021(9)	90	89.411(10)	90
V / Å^3	4291.5(11)	2566.8(3)	4724.9(19)	7004.4(10)	3646.2(13)	23653.0(16)
Z	2	1	2	2	2	8
T / K	150(2)	150(2)	150(2)	150(2)	150(2)	100(2)
D_c / g cm^{-3}	1.609	1.381	1.517	1.557	1.520	1.526
μ / mm^{-1}	1.282	1.075	1.195	1.280	0.762	1.561
□ range	3.639 - 25.682	3.977 - 25.027	3.644 – 27.485	3.540 - 25.027	3.698 - 25.027	2.149 - 24.191
Index ranges	-17 □ *h* □ 17 -17 □ *k* □ 17 -29 □ *l* □ 29	-16 □ *h* □ 16 -16 □ *k* □ 14 -17 □ *l* □ 17	-22 □ *h* □ 22 -21 □ *k* □ 22 -22 □ *l* □ 22	-17 □ *h* □ 17 -21 □ *k* □ 21 -31 □ *l* □ 31	-7 □ *h* □ 8 -22 □ *k* □ 22 -31 □ *l* □ 31	-28 □ *h* □ 28 -29 □ *k* □ 29 -32 □ *l* □ 32
Reflections collected	110715	20519	128931	109393	83856	226986
Independent reflections	16187 (R_{int} = 0.0604)	8395 (R_{int} = 0.0387)	21557 (R_{int} = 0.0292)	12298 (R_{int} = 0.0480)	12700 (R_{int} = 0.0386)	14570 (R_{int} = 0.0981)
Final *R* indices [I>2□(I)][a,b]	*R*1 = 0.0657 *wR*2 = 0.1539	*R*1 = 0.0974 *wR*2 = 0.2184	*R*1 = 0.0401 *wR*2 = 0.1134	*R*1 = 0.0986 *wR*2 = 0.2556	*R*1 = 0.0607 *wR*2 = 0.1179	*R*1 = 0.0803 *wR*2 = 0.1958
Final *R* indices (all data)	*R*1 = 0.0791 *wR*2 = 0.1623	*R*1 = 0.1143 *wR*2 = 0.2268	*R*1 = 0.0480 *wR*2 = 0.1227	*R*1 = 0.1046 *wR*2 = 0.2603	*R*1 = 0.0715 *wR*2 = 0.1221	*R*1 = 0.1065 *wR*2 = 0.2190
$(\Delta\rho)_{max,min}$ / e Å^{-3}	1.273 and -0.565	1.699 and -1.008	1.387 and -1.056	3.081 and -1.837	0.745 and -0.574	1.017 and -1.731

[a] $R1 = \sum(||F_o| - |F_c||)/\sum|F_o|$. [b] $wR2 = [\sum[w(F_o^2 - F_c^2)^2]/\sum[w(F_o^2)^2]]^{1/2}$, $w = 1/[\sigma^2(F_o^2) + [(ap)^2+bp]$, where $p = [\max(F_o^2, 0) + 2F_c^2]/3$.

Description of Structures

Complexes **1** and **2** are very similar to each other (Fig. 1) and differ only in the nature of the central μ_3-OR^- bridges (R = Me in **1** and R = H in **2**) and the terminally bound solvate molecules (MeOH in **1** and DMF in **2**). Therefore, only the structure of representative complex **2** will be described in detail. Selected interatomic distances and angles for all structurally and magnetically described compounds are listed in Tables 2-5. The crystallographically established coordination modes of the $nacb^{2-}$ ligands present in complexes **1**-**6** are shown in Scheme 2.

Complex **2** consists of 5 Ni^{II} cations held together by two μ_3-bridging OH^- ions (O1 and its symmetry equivalent), and two η^2:η^1:η^2:η^1:μ_4 (O2/O3/O4/N1 and their symmetry equivalents) and two η^1:η^1:η^2:μ (O5/O7/N2 and their symmetry equivalents) $nacb^{2-}$ ligands. Peripheral ligation is provided by four terminal DMF molecules, two on each of Ni2 and Ni2′ cations. The five Ni^{II} cations are disposed in a centered parallelogram, which is planar by virtue of a crystallographic inversion center in the middle (at Ni1). An alternative description of the metal topology of **2** (Fig. 2) is as two Ni^{II} triangles (Ni1-Ni2-Ni3 and Ni1-Ni2′-Ni3′) with a common vertex (a bowtie). Each triangle is nearly isosceles with the Ni1···Ni2, Ni1···Ni3 and Ni2···Ni3 distances being 3.057(3), 2.961(3) and 3.213(3) Å, respectively. The carboxylate O atoms of $nacb^{2-}$ serve to bridge the central Ni^{II} cation with the four peripheral ones. The bridging naphthoxido O atoms span the base (Ni2···Ni3 and Ni2′···Ni3′) of each isosceles triangle. Thus, the complete core of complex **2** is $[Ni_5(\mu_3\text{-}OH)_2(\mu_3\text{-}OOCR)_2(\mu\text{-}OR)_6]$, which includes the entire carboxylate moiety when this bridges through both O atoms (Fig. 2). Furthermore, Ni2 and Ni3 are bound to an O_5N set of donor atoms, while Ni1 forms a NiO_6 chromophore. Thus, all the Ni^{II} cations are six-coordinate with distorted octahedral geometry, with the

main distortion arising from the relatively small bite angles of the chelating parts of the nacb^{2-} groups. The bond distances around the Ni^{II} cations in **1** and **2** are typical of those found in octahedrally coordinated nickel(II) complexes with O and N ligation.[29] The bowtie-like topology seen in complexes **1** and **2** is of precedence in Ni^{II} cluster chemistry, especially in Ni/oximate cluster chemistry where diatomic N-O oximate bridges act as linkers between the central and peripheral Ni^{II} cations.[30]

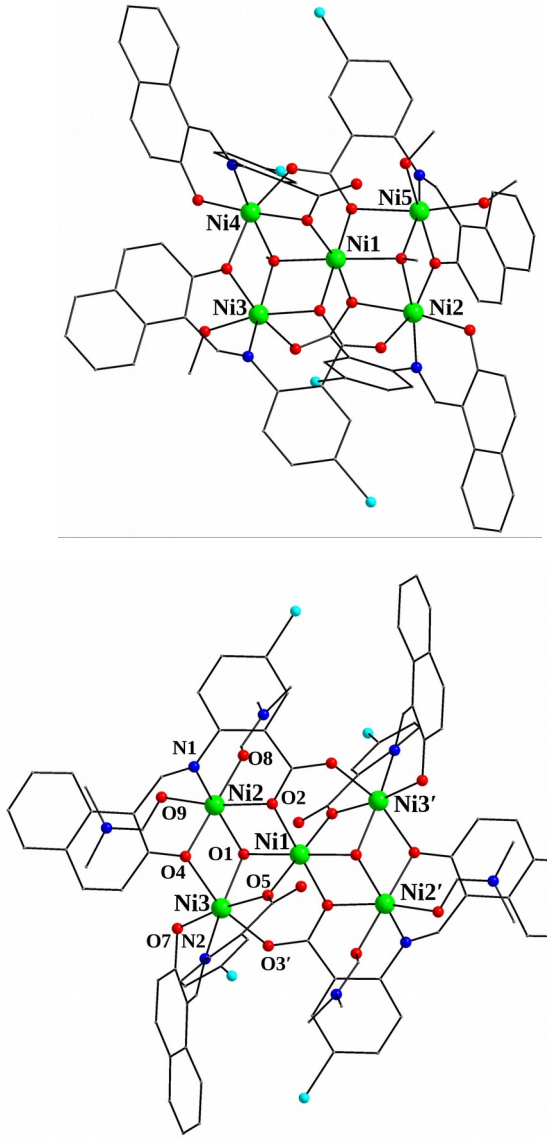

Fig. 1 Partially labeled plots of the Ni_5 molecules of **1** (top) and **2** (bottom). All H atoms are omitted for clarity. Primed and unprimed atoms are related by the crystallographic inversion center. Color scheme: Ni^{II} green, O red, N blue, C dark gray, Cl cyan.

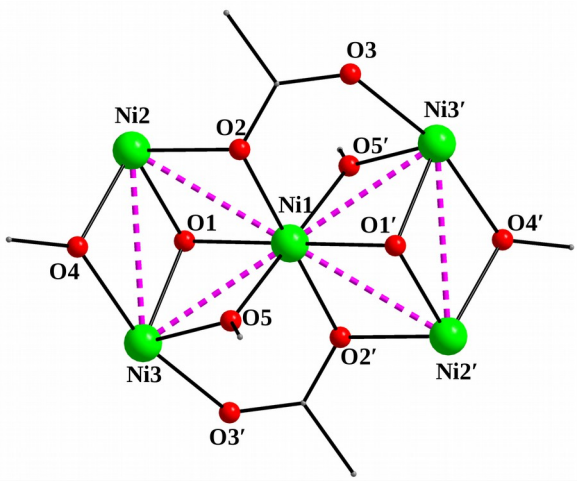

Fig. 2 The complete $[Ni_5(\mu_3\text{-}OH)_2(\mu_3\text{-}OOCR)_2(\mu\text{-}OR)_6]$ core of **2**; the purple dashed lines highlight the bowtie-like (or, alternatively, the two vertex-sharing triangular) topology.

Table 2 Selected interatomic distances (Å) and angles (°) for complex **2**[a]

Ni(1)-O(1)	2.044(4)	Ni(2)-N(1)	2.020(5)
Ni(1)-O(2)	2.056(4)	Ni(3)-O(1)	2.037(4)
Ni(1)-O(5)	2.017(4)	Ni(3)-O(3′)	2.121(4)
Ni(2)-O(1)	2.008(4)	Ni(3)-O(4)	2.173(4)
Ni(2)-O(2)	2.105(4)	Ni(3)-O(5)	2.028(5)
Ni(2)-O(4)	2.042(4)	Ni(3)-O(7)	2.001(5)
Ni(2)-O(8)	2.065(4)	Ni(3)-N(2)	2.043(6)
Ni(2)-O(9)	2.070(5)		
Ni(1)-O(1)-Ni(2)	98.0(2)	Ni(1)-O(5)-Ni(3)	94.1(2)
Ni(1)-O(2)-Ni(2)	94.6(2)	Ni(2)-O(1)-Ni(3)	105.2(2)
Ni(1)-O(1)-Ni(3)	93.1(2)	Ni(2)-O(4)-Ni(3)	99.3(2)

[a] Symmetry code: (′) = -x, -y, -z.

Table 3 Selected interatomic distances (Å) and angles (°) for complex **3**

Ni(1)-O(1)	2.069(2)	Ni(3)-O(11)	1.992(2)
Ni(1)-O(3)	2.086(2)	Ni(3)-O(13)	2.096(2)
Ni(1)-O(4)	2.084(2)	Ni(3)-N(2)	2.001(2)
Ni(1)-O(6)	2.117(2)	Ni(4)-O(3)	2.023(2)
Ni(1)-O(10)	2.030(2)	Ni(4)-O(4)	2.070(2)
Ni(1)-Cl(1)	2.350(7)	Ni(4)-O(13)	2.015(2)
Ni(2)-O(1)	2.033(2)	Ni(4)-O(14)	2.066(2)
Ni(2)-O(7)	2.045(2)	Ni(4)-N(3)	2.015(2)
Ni(2)-O(15)	1.988(2)	Ni(4)-N(4)	2.102(2)
Ni(2)-O(16)	2.086(2)	Ni(5)-O(5)	2.061(2)
Ni(2)-N(5)	2.015(2)	Ni(5)-O(6)	2.054(2)
Ni(2)-Cl(1)	2.443(8)	Ni(5)-O(8)	2.011(2)
Ni(3)-O(2)	2.090(2)	Ni(5)-O(9)	2.086(2)
Ni(3)-O(3)	2.053(2)	Ni(5)-O(12)	2.077(2)
Ni(3)-O(10)	2.038(2)	Ni(5)-N(1)	2.012(2)
Ni(1)-O(1)-Ni(2)	101.6(7)	Ni(1)-O(3)-Ni(4)	101.7(7)
Ni(1)-Cl(1)-Ni(2)	83.0(3)	Ni(1)-O(6)-Ni(5)	111.1(7)
Ni(1)-O(3)-Ni(3)	93.2(7)	Ni(3)-O(3)-Ni(4)	100.6(7)
Ni(1)-O(10)-Ni(3)	95.4(7)	Ni(3)-O(13)-Ni(4)	99.4(7)
Ni(1)-O(4)-Ni(4)	100.2(7)		

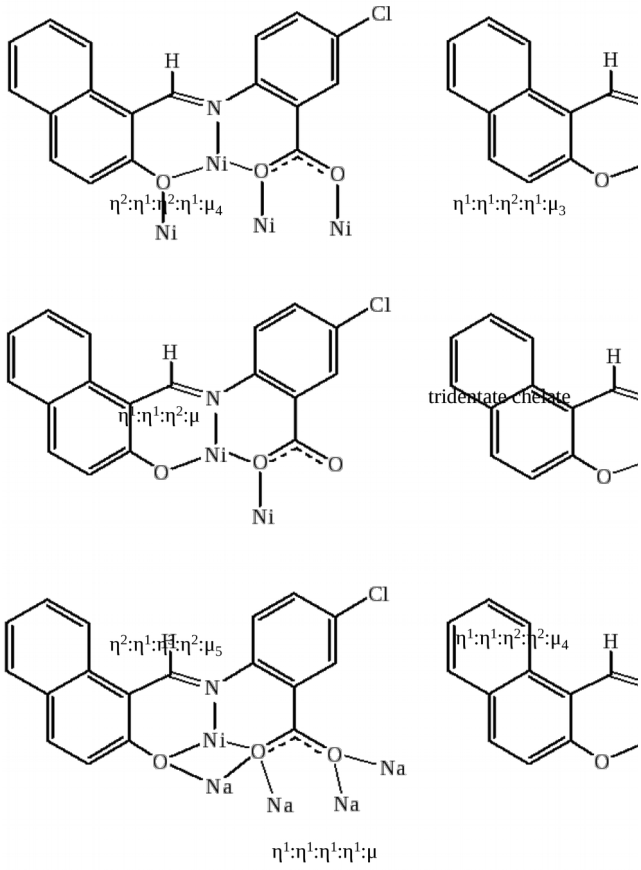

Scheme 2 Crystallographically established coordination modes of nacb^{2-} ligands present in complexes **1**-**6**.

Complex **3** comprises again five Ni^{II} cations (Fig. 3, top), but this time the metal ions are linked together by a μ_3-OMe$^-$, a μ-Cl$^-$, and the carboxylate and naphthoxido O atoms of four nacb^{2-} ligands to form an overall asymmetric, cage-like cluster. Three nacb^{2-} groups bind in an $\eta^1{:}\eta^1{:}\eta^2{:}\eta^1{:}\mu_3$ mode (Scheme 2), bridging solely through the carboxylate O atoms, and the remaining nacb^{2-} ligand adopts the more rare $\eta^2{:}\eta^1{:}\eta^2{:}\eta^1{:}\mu_4$ mode (Scheme 2), with the two 'pockets' of the ligand chelating a Ni^{II} cation and both the carboxylate and naphthoxido O atoms participating in the bridging of three additional metal ions. Thus, the complete core of **3** (including the triatomic carboxylate bridges from nacb^{2-}) is $[Ni_5(\mu_3\text{-OMe})(\mu\text{-Cl})(\mu_3\text{-OOCR})_4(\mu\text{-OR})]^{3+}$ (Fig. 3, bottom) and can be conveniently described as a $\{Ni_3(\mu_3\text{-OMe})\}$ triangle bridged to two additional Ni^{II} cations through the bridging carboxylate moieties of nacb^{2-} and the bridging chloride group. Such a structural motif is unprecedented in Ni^{II} cluster chemistry. Peripheral ligation about the core is provided by three terminal MeOH (on Ni2, Ni4 and Ni5) and a terminal MeCN (on Ni4) molecules. The Ni-Cl bond distances (Ni1···Cl1 = 2.351(2) Å and Ni2···Cl1 = 2.443(2) Å) fall into the expected range for similar μ-Cl$^-$-bridged Ni^{II} compounds.[31] All Ni^{II} cations in **3** are six-coordinate with distorted octahedral geometries.

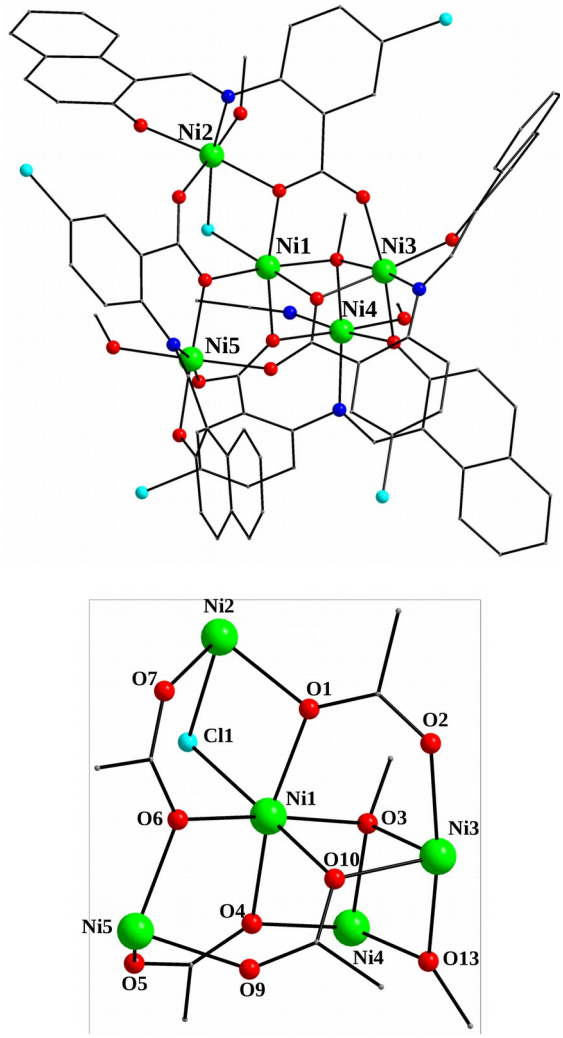

Fig. 3 (top) Partially labeled representation of the structure of **3** and (bottom) its complete $[Ni_5(\mu_3\text{-OMe})(\mu\text{-Cl})(\mu_3\text{-OOCR})_4(\mu\text{-OR})]^{3+}$ core. All H atoms are omitted for clarity. Color scheme as in Fig. 1.

The crystal structure of complex **4** consists of $[Ni_6(OH)_2(nacb)_6(H_2O)_4]^{2-}$ anions (Fig. 4, top) counterbalanced by $NHEt_3^+$ cations; the latter, as well as the six CH_2Cl_2 lattice solvate molecules, will not be further discussed. The Ni_6 anion consists of a central, planar array of four Ni^{II} cations, or alternatively a Ni_4 rod-like unit, comprising Ni1, Ni3, Ni1′ and Ni3′, which is further linked to two Ni^{II} cations (Ni2 and Ni2′) via two μ_3-OH$^-$ ions. Two nacb^{2-} ligands act as tridentate chelates on Ni2 and Ni2′, while the remaining four nacb^{2-} ligands behave as both tridentate chelating and bridging groups, adopting the $\eta^1{:}\eta^1{:}\eta^2{:}\eta^1{:}\mu_3$ mode (Scheme 2). Four water molecules occupy the terminal coordination sites of Ni1 and Ni1′. Hence, all Ni^{II} cations are again six-coordinate with distorted octahedral geometries but with different NiO_xN_y chromophores (x = 6, y = 0 for Ni1/Ni1′; x = 5, y = 1 for Ni2/Ni2′; x = 4, y = 2 for Ni3/Ni3′). The complete core of **4** is $[Ni_6(\mu_3\text{-OH})_2(\mu_3\text{-OOCR})_4]^{6+}$ (Fig. 4, bottom), and can also be seen as a $\{Ni_4(\mu_3\text{-OH})_2\}$ butterfly in the center of the cluster attached to two extrinsic Ni^{II} cations on both sides. Complex **4** exhibits a rather unusual topology among the hundreds of structurally characterized Ni$^{II}_6$ clusters to date; only the ferromagnetically-coupled complex

$(NHEt_3)_2[Ni_6(OH)_2(L)_4(H_2O)_2]$ (LH_3 = 2,2′,2″-nitrilotribenzoic acid) reported by Krämer and co-workers has shown a similar metal topology.[32]

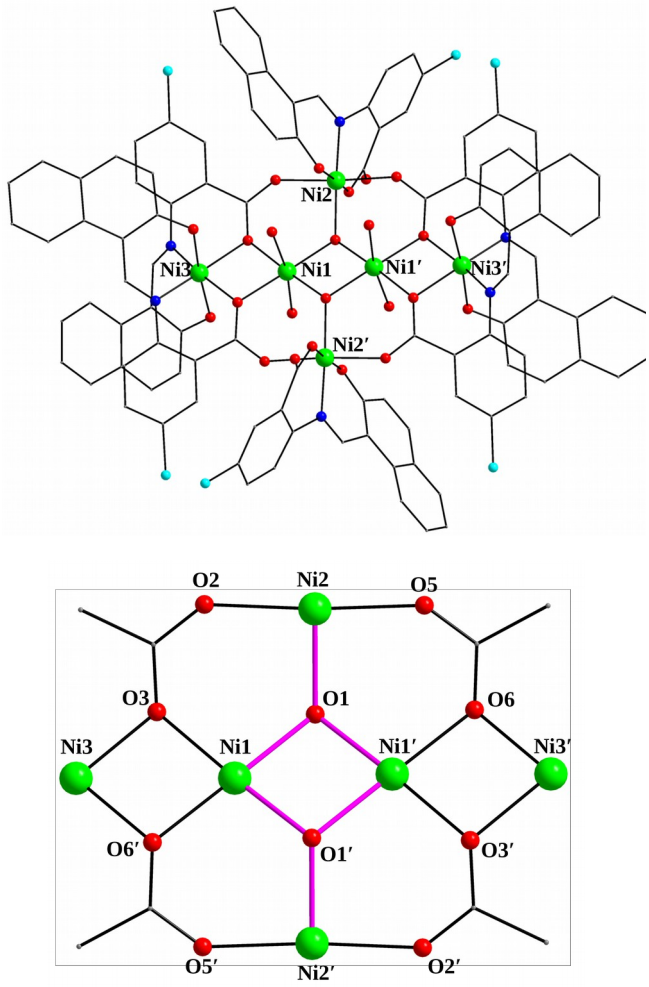

Fig. 4 (top) Labeled plot of the $[Ni_6(OH)_2(nacb)_6(H_2O)_4]^{2-}$ anion of complex **4** and (bottom) its complete core, with the purple colored bonds indicating the $\{Ni_4(\mu_3\text{-}OH)_2\}$ butterfly unit. Color scheme as in Fig. 1. H-atoms are omitted for clarity. Primed atoms are related to the non-primed ones by the symmetry operation: 2-*x*, -*y*, -*z*.

Table 4 Selected interatomic distances (Å) and angles (°) for complex **4**[a]

Ni(1)-O(1)	2.028(5)	Ni(2)-O(8)	2.017(5)
Ni(1)-O(1′)	2.026(5)	Ni(2)-O(10)	2.018(5)
Ni(1)-O(3)	2.090(5)	Ni(2)-N(3)	2.021(6)
Ni(1)-O(6′)	2.080(5)	Ni(3)-O(3)	2.075(5)
Ni(1)-O(11)	2.081(5)	Ni(3)-O(4)	2.022(5)
Ni(1)-O(12)	2.099(5)	Ni(3)-O(6′)	2.054(5)
Ni(2)-O(1)	2.025(5)	Ni(3)-O(7′)	2.054(5)
Ni(2)-O(2)	2.118(5)	Ni(3)-N(1)	2.007(6)
Ni(2)-O(5)	2.095(5)	Ni(3)-N(2′)	2.013(6)
Ni(1)-O(1)-Ni(1′)	95.9(2)	Ni(1)-O(3)-Ni(3)	93.1(2)
Ni(1)-O(1)-Ni(2)	124.6(2)	Ni(1)-O(6′)-Ni(3)	94.0(2)
Ni(1)-O(1′)-Ni(2′)	121.4(2)		

[a] Symmetry code: (′) = 2-*x*, -*y*, -*z*.

The crystal of **5** contains two co-crystallized $\{NiNa_2\}$ coordination polymers with very similar formulas and both with one-dimensional motifs. The $[NiNa_2(nacb)_2(MeOH)_2]_n$ (**5a**) and $[NiNa_2(nacb)_2(MeOH)_2(H_2O)_2]_n$ (**5b**) polymers differ only in the presence of two terminally ligated water molecules on the Na^I cations of **5b**. Due to several disorders located on many atoms within **5b**, the structure of **5a** will be described in detail as a representative example. The asymmetric unit of **5a** (Fig. 5, top) comprises a distorted octahedral Ni^{II} cation (Ni1) surrounded by two tridentate chelating $nacb^{2-}$ groups. Within the asymmetric unit, one of the $nacb^{2-}$ ligands utilizes one carboxylate O atom (O4) to bridge Ni1 with two Na^I cations (Na1 and Na2). The latter are additionally bound to two terminal MeOH molecules (O7 and O8). Subsequently, one of the bound MeOH molecules (the one containing O7) becomes μ-bridging and connects Na1 with the symmetry related Na1′ (′ = 1-*x*, -*y*, -*z*). In addition, O5 from the carboxylate fragment of $nacb^{2-}$ becomes μ-bridging and links Ni1 with Na1′; this ligand is thus bridging in an overall $\eta^1{:}\eta^1{:}\eta^2{:}\eta^2{:}\mu_4$ mode (Scheme 2). The behavior of the second bridging $nacb^{2-}$ ligand is slightly more complex; the naphthoxido O atom, O1, bridges Ni1 with Na2″ (″ = 1+*x*, *y*, *z*), while the carboxylate O atoms (O2 and O3) demonstrate a noticeable bridging ability, linking Ni1 to four additional Na^I cations (Na1′, Na2″ for O2 and Na1″, Na2′ for O3). This ligand is thus bridging in an overall $\eta^2{:}\eta^1{:}\eta^3{:}\eta^2{:}\mu_5$ mode (Scheme 2), which is unprecedented in the coordination chemistry of $nacb^{2-}$ to date. The activation of all symmetry elements and operations within the extended structure of **5a** (Fig. 5, middle) reveals the complete 1-D chain which is shown in the bottom of Fig. 5. The Na1 and Na2 cations have very distorted octahedral and square pyramidal coordination geometries, respectively. The τ index for Na2 was calculated as 0.22, where τ is 0 and 1 for perfect square pyramidal and trigonal bipyramidal geometries,[33] respectively. Finally, the Ni···Ni distances in **5a** are within the range 7.551(3)-8.199(3) Å, thus presaging negligible magnetic exchange interactions between the paramagnetic metal ions.

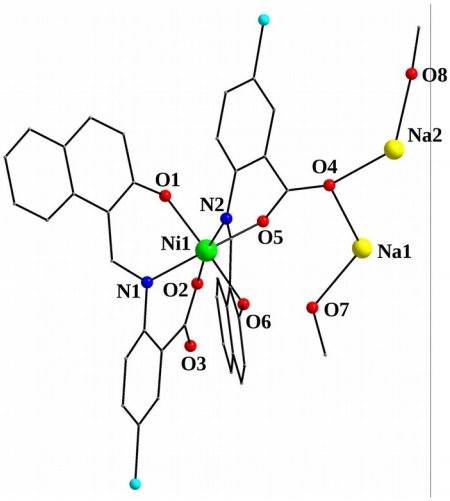

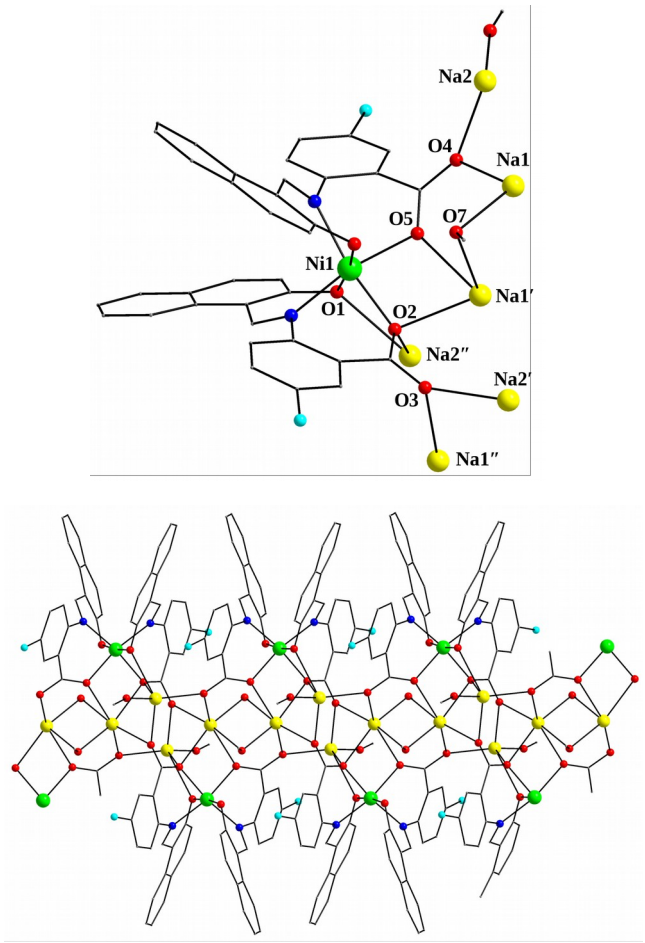

Fig. 5 (top) Labeled representation of the asymmetric unit of **5a** and (middle) its extended structure. (bottom) A small portion of the 1-D chain structure of **5a** along the crystallographic *c* axis. Color scheme as in Fig. 1; Na^{i} yellow. H-atoms are omitted for clarity. Single- and double-primed atoms are related to the non-primed ones by the symmetry operations: 1-*x*, -*y*, -*z* and 1+*x*, *y*, *z*, respectively.

The crystal structure of complex **6** contains hexanuclear $[Ni_6(nacb)_6(H_2O)_3(MeOH)_6]$ clusters (Fig. 6, top) and CH_2Cl_2 and H_2O lattice solvate molecules; the latter two will not be further discussed. The formula of **6** is charge-balanced and comprises six distorted octahedral Ni^{II} cations bridged together by three μ-bridging H_2O molecules and the carboxylate fragments of six $nacb^{2-}$ ligands. Six MeOH molecules complete the coordination spheres of the six Ni^{II} cations. The $nacb^{2-}$ ligands are all acting as $\eta^1{:}\eta^1{:}\eta^1{:}\eta^1{:}\mu$ bridging groups (Scheme 2), another new coordination mode for this class of ligands, with the imino N and naphthoxido O atoms chelating a Ni^{II} cation and the carboxylate O atoms bridging that Ni^{II} with a neighboring one in a *syn*,*anti*-bridging fashion. Although rare, the bridging capacity of H_2O molecules in Ni^{II} cluster chemistry is of precedence.[34] Metric parameters and O bond valence sum (BVS)[35] calculations further supported the assignment of these O atoms to H_2O molecules. The O BVS values for O1W, O2W and O3W in **6** were 0.64, 0.64 and 0.67, respectively; an O BVS in the ~0.2-0.8 range is indicative of double protonation. The Ni-O_{aqua} distances are larger than the Ni-$O_{naphthoxido}$ and Ni-$O_{carboxylate}$ ones, as expected for bridging aqua groups. The core of **6** is thus $[Ni_6(\mu\text{-}O_2H)_3(\mu\text{-}OOCR)_6]^{6+}$ (Fig. 6, bottom) and can be described as three interpenetrating $\{Ni_2(\mu\text{-}O_2H)\}$ units (Ni1-O1W-Ni2, Ni3-O2W-Ni4 and Ni5-O3W-Ni6) bridged to each other by the *syn*,*anti*-$\eta^1{:}\eta^1{:}\mu$ carboxylate groups of the $nacb^{2-}$ ligands. This asymmetric metal core topology has not been reported to date in Ni_6 cluster chemistry.

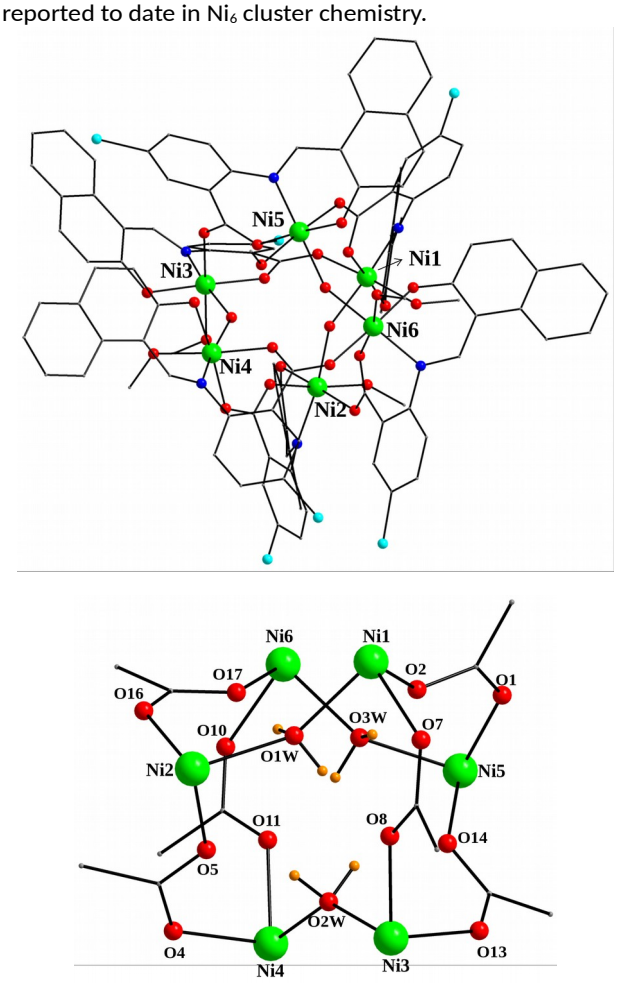

Fig. 6 (top) Partially labeled representation of the structure of **6** and (bottom) its complete $[Ni_6(\mu\text{-}O_2H)_3(\mu\text{-}OOCR)_6]^{6+}$ core. H atoms are either omitted for clarity or shown in orange color. Color scheme for the remaining atoms as in Fig. 1.

Table 5 Selected interatomic distances (Å) and angles (°) for complex **6**

Ni(1)-O(1W)	2.088(6)	Ni(4)-O(2W)	2.069(6)
Ni(1)-O(2)	1.999(6)	Ni(4)-O(4)	2.064(7)
Ni(1)-O(3)	1.977(6)	Ni(4)-O(11)	2.059(7)
Ni(1)-O(7)	2.075(6)	Ni(4)-O(12)	2.011(6)
Ni(1)-O(19)	2.103(6)	Ni(4)-O(22)	2.077(7)
Ni(1)-N(1)	1.962(7)	Ni(4)-N(4)	1.973(8)
Ni(2)-O(1W)	2.099(6)	Ni(5)-O(1)	2.100(6)
Ni(2)-O(5)	2.028(6)	Ni(5)-O(3W)	2.073(6)
Ni(2)-O(6)	2.008(7)	Ni(5)-O(14)	1.998(7)
Ni(2)-O(16)	2.080(7)	Ni(5)-O(15)	1.999(7)
Ni(2)-O(20)	2.061(6)	Ni(5)-O(23)	2.085(6)
Ni(2)-N(2)	1.980(9)	Ni(5)-N(5)	1.978(8)
Ni(3)-O(2W)	2.112(6)	Ni(6)-O(3W)	2.080(6)
Ni(3)-O(8)	1.987(6)	Ni(6)-O(10)	2.087(7)
Ni(3)-O(9)	1.974(7)	Ni(6)-O(17)	2.051(7)
Ni(3)-O(13)	2.099(6)	Ni(6)-O(18)	1.988(7)
Ni(3)-O(21)	2.087(7)	Ni(6)-O(24)	2.048(7)
Ni(3)-N(3)	1.982(8)	Ni(6)-N(6)	1.999(8)
Ni(1)-O(1W)-Ni(2)	137.7(3)	Ni(5)-O(3W)-Ni(6)	137.6(3)
Ni(3)-O(2W)-Ni(4)	138.7(3)		

Intramolecular and Intermolecular Interactions

The intermolecular interactions in all the reported compounds **1**-**6** are very weak to negligible and do not merit any further discussion. In contrast, there are some interesting intramolecular H-bonding interactions in **1**-**6** which deserve to be further discussed; these interactions provide the systems with additional thermodynamic stability and allow them to crystallize under normal conditions. In the crystal structures of complexes **1** and **3**, there are strong intramolecular H bonds between the terminally bound MeOH molecules, the naphthoxido O atoms of nacb^{2-} and the lattice solvate MeOH molecules. In complex **2**, the μ_3-OH$^-$ groups are found to be H-bonded with the uncoordinated carboxylate O atoms of nacb^{2-}. In the crystal structure of complex **4**, there are two sets of different H-bonding interactions; these are between the naphthoxido O atoms of the tridentate chelating nacb^{2-} ligands and the terminally bound H_2O molecules, and between the uncoordinated carboxylate O atoms of nacb^{2-} and the $NHEt_3^+$ countercations. Within each of the two polymers **5a** and **5b**, there are only H-bonding interactions between the naphthoxido O atoms of nacb^{2-} and the bridging MeOH groups. Finally, the crystal structure of complex **6** exhibits a very rich network of intramolecular H-bonding interactions (Fig. 7, Table 6). In particular, each of the bridging H_2O molecules is H bonded to two carboxylate O atoms from two different nacb^{2-} ligands. Furthermore, all six terminal MeOH molecules are H-bonded to the naphthoxido O atoms of six different nacb^{2-} ligands.

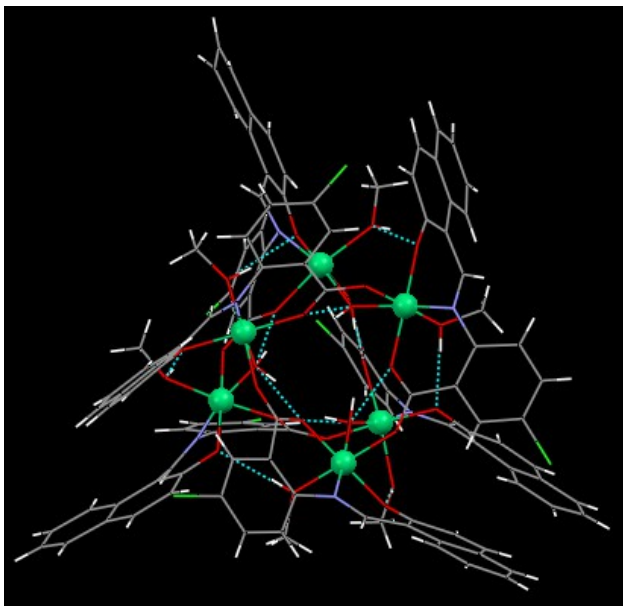

Fig. 7 The intramolecular H bonds (blue dashed lines) that are present in the crystal structure of **6**. H atoms are shown in white.

Table 6 Intramolecular hydrogen bonds in the crystal structure of complex **6** (A = acceptor, D = donor)

Interaction	D···A (Å)	H···A (Å)	D-H···A (°)
O(1W)-H(1W)···O(8)	2.672(8)	1.87	156.1
O(1W)-H(2W)···O(17)	2.607(9)	1.78	163.9
O(2W)-H(5W)···O(14)	2.685(8)	1.94	141.7
O(2W)-H(6W)···O(5)	2.623(8)	1.79	159.5
O(3W)-H(3W)···O(2)	2.659(8)	1.86	153.0
O(3W)-H(4W)···O(11)	2.609(8)	1.78	156.6
O(19)-H(19)···O(18)	2.739(10)	1.95	155.0
O(20)-H(20)···O(3)	2.645(8)	1.81	171.7
O(21)-H(21A)···O(6)	2.719(9)	1.95	152.1
O(22)-H(22)···O(9)	2.653(10)	1.81	176.1
O(23)-H(23)···O(12)	2.716(10)	1.90	163.3
O(24)-H(24)···O(15)	2.616(10)	1.80	165.2

Solid-state Magnetic Susceptibility Studies

Variable-temperature (2.0-300 K range), direct-current (dc) magnetic susceptibility measurements were performed on freshly-prepared microcrystalline solids of **2**, **3**·MeCN, **4** and **6**·H_2O; a dc field of 0.3 T was applied from 30 to 300 K and a weak dc field of 0.03 T was used from 2 to 30 K to avoid saturation effects. The magnetic behavior of complex **1** was similar to that of the isostructural complex **2**. The magnetic properties of the coordination polymer **5** were not further elucidated since **5** can be magnetically considered as a single Ni^{II} monomer comprising non-interacting paramagnetic metal ions. The data of all studied compounds are shown as $\chi_M T$ *vs*. *T* plots in Fig. 8. Scheme 3 shows the numbering scheme of the spin carriers that was employed for the discussion of the magnetic properties of all compounds, including the analysis of the applied spin Hamiltonians, the corresponding fits of the data, and the attempted magnetostructural correlations between the calculated *J* coupling constants and the types of different superexchange pathways.

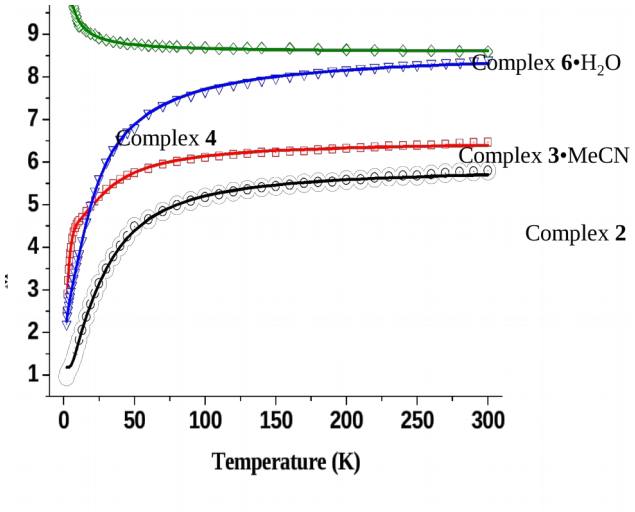

Fig. 8 $\chi_M T$ *vs.* *T* plots for complexes **2**, **3**·MeCN, **4** and **6**·H_2O. The solid lines are the fits of the data; see the text for the spin Hamiltonians and the corresponding fit parameters.

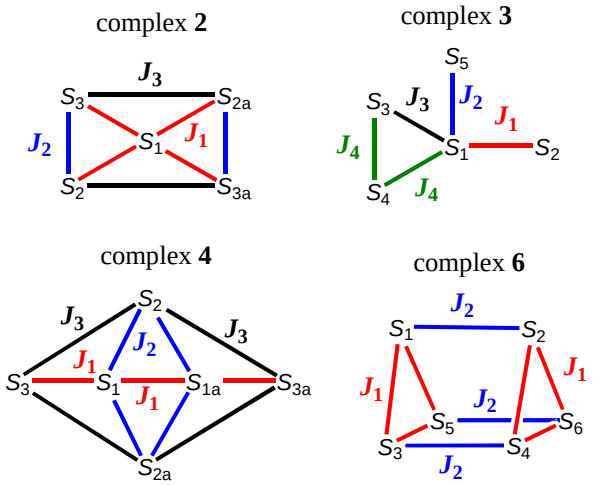

Scheme 3 *J*-coupling scheme employed for the elucidation of the magnetic exchange interactions in complexes **2**, **3**, **4** and **6**.

For the $[Ni_5(OH)_2(nacb)_4(DMF)_4]$ complex (**2**), the $\chi_M T$ product steadily decreases with decreasing *T*, from a value of 5.80 $cm^3mol^{-1}K$ at 300 K to 0.97 $cm^3mol^{-1}K$ at 2 K; such behavior is consistent with the presence of predominant antiferromagnetic exchange interactions between the five Ni^{II} cations. The $\chi_M T$ value at 2 K is very close to the expected one (1 $cm^3mol^{-1}K$ with g = 2) for an S = 1 spin ground state. There are eight interaction pathways in total within **2**; these can be further simplified to three (Scheme 3) considering the symmetry of the cluster and the types of bridges involved in the superexchange mechanism. The complete spin Hamiltonian for **2** is given by eq. 1.

$$H = -J_1(\hat{S}_1\cdot\hat{S}_2 + \hat{S}_1\cdot\hat{S}_3 + \hat{S}_1\cdot\hat{S}_{2a} + \hat{S}_1\cdot\hat{S}_{3a}) - J_2(\hat{S}_2\cdot\hat{S}_3 + \hat{S}_{2a}\cdot\hat{S}_{3a}) - J_3(\hat{S}_2\cdot\hat{S}_{3a} + \hat{S}_{2a}\cdot\hat{S}_3) \quad (1)$$

The best-fit parameters were: J_1 = -0.9 cm^{-1}, J_2 = -13.6 cm^{-1}, J_3 = -1.8 cm^{-1} and g = 2.20 (R = 3.2 × 10^{-5}). As a result, the spin ground state of **2** is S = 1 with the first excited state being 9.9 cm^{-1} higher in energy. The values of the calculated *J*-coupling constants are consistent with the structural features of complex **2** and the associated metric parameters; thus, the dominant antiferromagnetic interactions observed in **2** are attributed to the large Ni-O-Ni bond angles which span the range 93.1(2)-105.2(2)°.[8,28-32,34,36] Magnetization *vs.* field data (Fig. 9) were collected at 2 K and the experimental results were nicely reproduced for an isolated S = 1 ground state with a g value of 2.10 and a D value of 1.6 cm^{-1} (R = 2.2 × 10^{-4}), where D is the ground state zero-field splitting parameter.

The $\chi_M T$ product of the $[Ni_5(OMe)Cl(nacb)_4(MeOH)_3(MeCN)]$ (**3**) complex is again steadily decreasing as the temperature decreases and it reaches a value of 2.50 $cm^3mol^{-1}K$ at 2 K. The room temperature $\chi_M T$ value is 6.46 $cm^3mol^{-1}K$, slightly larger than the expected $\chi_M T$ value (6.05 $cm^3mol^{-1}K$ with g = 2.2) for five non-interacting Ni^{II} cations. The shape of the $\chi_M T$ *vs.* *T* plot indicates predominant antiferromagnetic exchange interactions between the metal ions. Due to the asymmetry of the cage-like **3**, there appears to be a very complicated pattern of interactions in which all nickel cations are magnetically connected to each other through different superexchange pathways. To simplify the fit and avoid overparameterization effects, we have discarded the *a priori* weaker magnetic interactions mediated by the *syn,syn*- or *syn,anti*-RCO_2^- bridges.[14,36] We have also employed the same *J*-coupling constant to describe the interactions between the Ni1•••Ni4 and Ni3•••Ni4 pairs within the near isosceles Ni1-Ni3-Ni4 triangle (Ni1•••Ni3 = 3.009 Å, Ni3•••Ni4 = 3.137 Å and Ni1•••Ni4 = 3.186 Å); the latter interactions are propagated by double-alkoxido bridges. The simplified 4-*J* spin Hamiltonian for **3** is given by eq. 2.

$$H = -J_1(\hat{S}_1\cdot\hat{S}_2) - J_2(\hat{S}_1\cdot\hat{S}_5) - J_3(\hat{S}_1\cdot\hat{S}_3) - J_4(\hat{S}_1\cdot\hat{S}_4 + \hat{S}_3\cdot\hat{S}_4) \quad (2)$$

We have included in the fitting model a D_{ion} term in order to reproduce adequately the magnetic data at the low-temperature regime. An excellent fit of the data was obtained for the entire temperature region, including the region of the plot where the shape of the curve is slightly different (i.e., steeper decrease between 75 and 10 K). The best-fit parameters were: J_1 = -0.8 cm^{-1}, J_2 = +12.2 cm^{-1}, J_3 = +2.0 cm^{-1}, J_4 = -13.1 cm^{-1}, D_{ion} = -2.5 cm^{-1} and g = 2.28 (R = 2.6 × 10^{-5}). Using the same fit parameters, we have also been able to simulate the magnetization *vs.* field data (Fig. 9). Even with this simplified spin Hamiltonian, the fitting model still includes a large number of parameters and therefore their absolute values should be taken as indicative only. However, the two main interactions associated with J_4 and J_2 coupling constants are fully consistent with the expected antiferromagnetic coupling mediated by the double alkoxido bridges with large Ni-O-Ni bond angles (99.4(7)-101.6(7)°)[36] and the ferromagnetic coupling resulted from the small Ni1-Cl1-Ni2 bond angle (83.0(3)°),[34] respectively. Hence, the calculated ground state from the obtained fit parameters is S = 1 but -in contrast to the Ni_5 complex **2**- the ground state this time is

close in energy with the low-lying S = 2 and 3 excited states. The population of these excited states, with S larger than that of the ground state, under large magnetic fields forces the magnetization to reach a value of 5.7 Nμ_B (Fig. 9).

The $\chi_M T$ product of the $(NHEt_3)_2[Ni_6(OH)_2(nacb)_6(H_2O)_4]$ (**4**) complex decreases monotonically from 8.39 $cm^3mol^{-1}K$ at 300 K to 2.19 $cm^3mol^{-1}K$ at 2 K. The room temperature $\chi_M T$ value is smaller than the expected one for six non-interacting Ni^{II} cations (7.26 $cm^3mol^{-1}K$ with g = 2.2). The shape of the plot indicates again predominant antiferromagnetic exchange interactions between the metal ions. This system also shows a complicated pattern of twelve interactions in total, which can be simplified to the below 3-J spin Hamiltonian (eq. 3) on the basis of the structural features and metric parameters of complex **4**.

$$H = -J_1(\hat{S}_1\cdot\hat{S}_3 + \hat{S}_1\cdot\hat{S}_{1a} + \hat{S}_{1a}\cdot\hat{S}_{3a}) - J_2(\hat{S}_1\cdot\hat{S}_2 + \hat{S}_{1a}\cdot\hat{S}_2 + \hat{S}_1\cdot\hat{S}_{2a} + \hat{S}_{1a}\cdot\hat{S}_{2a}) - J_3(\hat{S}_2\cdot\hat{S}_3 + \hat{S}_2\cdot\hat{S}_{3a} + \hat{S}_{2a}\cdot\hat{S}_3 + \hat{S}_{2a}\cdot\hat{S}_{3a}) \quad (3)$$

The best-fit parameters were: J_1 = -1.8 cm^{-1}, J_2 = -6.4 cm^{-1}, J_3 = -0.8 cm^{-1}, D_{ion} = 1.0 cm^{-1} and g = 2.30 (R = 2.7 × 10^{-5}). The mean Ni-O-Ni angles for the different Ni•••Ni pairs described by J_1 and J_2 in **4** (see Scheme 3 and Fig. 4, bottom) are 94.3° and 123.0°, respectively; thus, J_2 is expected to be the most antiferromagnetic, and indeed, it is. With regards to the J_3 coupling constant, this accounts for the magnetic interactions promoted solely by the long carboxylate bridges; these interactions are expected to be very weak and this is indeed the case as demonstrated by the fit of the data. From the obtained J-coupling constants, an S = 2 ground state was calculated. However, the fit of the magnetization data, assuming an isolated S = 2 ground state, was not completely satisfactorily; the quasi saturated value of 4.3 Nμ_B for the magnetization at large fields (Fig. 9) may be tentatively ascribed to the same S = 2 ground state as calculated from the magnetic susceptibility data.

In contrast to all previously studied compounds, the magnetic behavior of complex $[Ni_6(nacb)_6(H_2O)_3(MeOH)_6]$ (**6**) is completely different. The $\chi_M T$ product steadily increases with decreasing temperature from a value of 8.59 $cm^3mol^{-1}K$ at 300 K to a maximum value of 10.09 $cm^3mol^{-1}K$ at 3 K, thus suggesting the presence of predominant ferromagnetic exchange interactions between the metal ions. The room temperature $\chi_M T$ value is larger than the expected one for six non-interacting Ni^{II} cations. The structural data indicate the presence of two different types of superexchange pathways; one pathway results from the *syn*,*anti*-carboxylate bridges (attributed to J_1) and the other one is mediated by the μ-H_2O (assigned to J_2) bridges (see Fig. 6, bottom and Scheme 3). As a result, a 2-J spin Hamiltonian was employed (eq. 4) in order to fit the experimental data.

$$H = -J_1(\hat{S}_1\cdot\hat{S}_3 + \hat{S}_1\cdot\hat{S}_5 + \hat{S}_3\cdot\hat{S}_5 + \hat{S}_2\cdot\hat{S}_4 + \hat{S}_2\cdot\hat{S}_6 + \hat{S}_4\cdot\hat{S}_6) - J_2(\hat{S}_1\cdot\hat{S}_2 + \hat{S}_3\cdot\hat{S}_4 + \hat{S}_5\cdot\hat{S}_6) \quad (4)$$

An initial isotropic fit of the experimental data did not yield any satisfactory results but the incorporation of a D_{ion} term led to an excellent fit with parameters: J_1 = +0.3 cm^{-1}, J_2 = -0.1 cm^{-1}, D_{ion} = -1.3 cm^{-1} and g = 2.29 (R = 1.2 × 10^{-5}). The obtained -small in magnitude- J values are consistent with the expected values derived from two superexchange pathways that are known to promote very weak magnetic coupling; this coupling is often ferromagnetic for the single *syn*,*anti*-carboxylates,[37] and practically negligible for aqua bridges,[34] in agreement with the corresponding J_1 and J_2 values of **6**. Magnetization *vs.* field measurements were performed at 2 K. At the higher magnetic fields employed, the magnetization shows a non-saturated value of 8.8 Nμ_B. This value can be attributed to the presence of weak antiferromagnetic components in **6**; a fit of the data was not performed due to the large number of parameters involved and their very small values which would allow for the calculation of multiple solutions.

Finally, none of the reported compounds exhibit out-of-phase (imaginary) *ac* magnetic susceptibility signals down to 1.8 K, suggesting these are not SMMs.

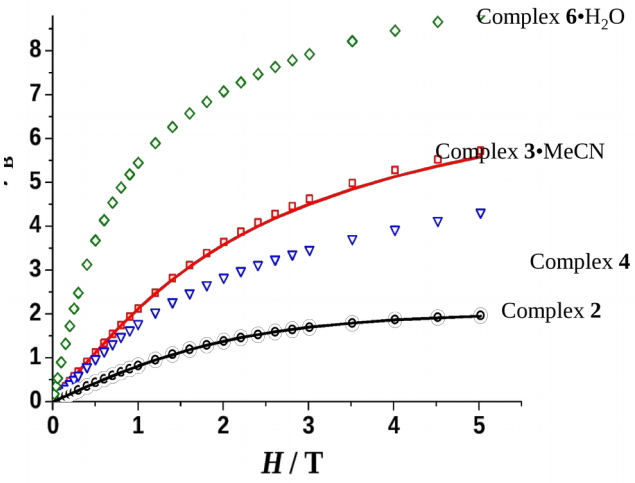

Fig. 9 Plots of magnetization (M) *vs.* field (H) for complexes **2**, **3**, **4** and **6**·H_2O at 2 K. The solid lines are the fits of the data for complexes **2** and **3** using the parameters discussed in the text.

Solid-State Emission Studies

The photophysical properties of complexes **1**-**6** were studied in the solid-state and at room temperature due to their structural degradation in solution. The latter was confirmed by performing ESI-MS studies in solutions of all complexes at various solvent media. These studies revealed -for all compounds- the presence of various high-intensity signals corresponding to different nuclearity species of similar abundance, including peaks which were assigned to ligand dissociation from the metal ions. The optical response of the free-ligand $nacbH_2$ has been reported in a previous work.[14] Briefly, it was shown that $nacbH_2$ is a promising 'antenna' group for the promotion of energy transfer effects. Upon maximum excitation at 349 nm, $nacbH_2$ exhibits a strong emission in the 380-420 nm visible range with two clear maxima at 391 and 410 nm, and a weak shoulder at 482 nm. Among all the studied Ni^{II} complexes, only **2** and **6** showed a noticeable photophysical response, which was similar in terms of excitation/emission peak maxima but with different intensities. The pentanuclear complex **2** exhibits a green-centered emission

at 544 nm, upon maximum excitation at 399 nm (Fig. 10, top), while the hexanuclear complex **6** shows a similar emission at 520 nm upon maximum excitation at 380 nm (Fig. 10, bottom). The emissions of both **2** and **6** are very red-shifted with respect to the free nacbH$_2$; this can be tentatively assigned to the coordination of the deprotonated nacb^{2-} ligands with the metal ions which would subsequently affect the charge transfer process and eventually the detected emissions.[38]

It is now well-known that the deprotonation and coordination of a ligand to a metal ion enhances the rigidity of the organic molecule and consequently reduces the loss of energy via vibrational motions.[38] It has also been seen that the employment of efficient organic fluorescent ligands, such as those containing poly-aromatic rings (i.e., naphthalene, anthracene, phenanthrene, etc.), can prevent quenching effects induced by the paramagnetic nature of the metal ions.[38c,38d] Red-shifted emissions are usually observed in the majority of fluorescent compounds in the solid-state probably due to the π-π stacking interactions of the aromatic rings of the molecules.[13] Given the structural complexity of **2** and **6**, the number of metal ions and ligands present, among other structural perturbations (i.e., bound- and lattice-solvate molecules), an in-depth analysis of the photophysical energy transfer process was not feasible.

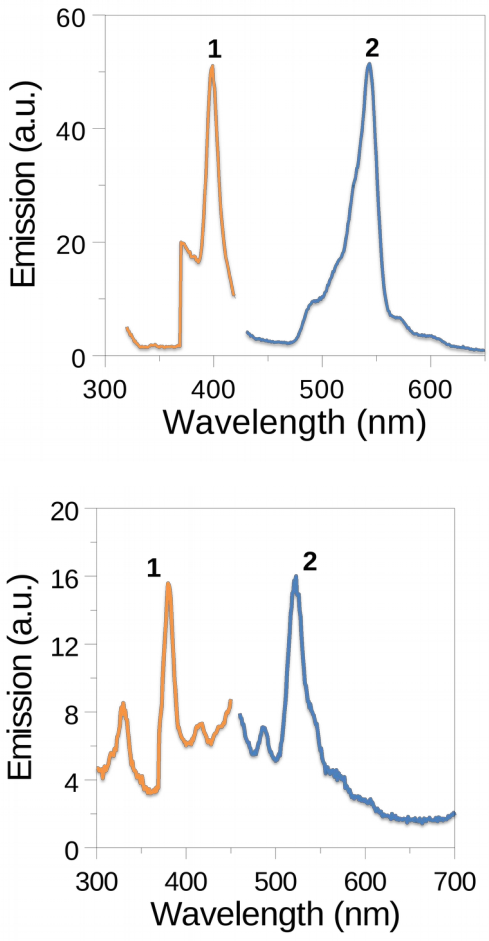

Fig. 10 Excitation (1) and emission (2) spectra of complexes **2** (top) and **6** (bottom) in the solid-state and at room temperature.

Conclusions

In conclusion, we have herein reported our results from the use of a flexible reaction scheme comprising the organic chelating/bridging ligand *N*-naphthalidene-2-amino-5-chlorobenzoic acid (nacbH$_2$) and simple Ni^{II} starting materials, in the presence of various organic or inorganic bases and at various solvent media. A series of structurally, magnetically and optically different pentanuclear and hexanuclear Ni^{II} cluster compounds, as well as a {NiNa$_2$}$_n$ coordination polymer, were obtained as a result of the bridging versatility, coordination affinity and optical efficiency of the deprotonated nacb^{2-} group. In addition, the nature of the base employed for the deprotonation of the free nacbH$_2$ and the reaction solvent were found to affect dramatically the chemical and structural identities of the resulting compounds. We are currently trying to expand this research into various Ni^{II} carboxylate sources as a means of increasing the nuclearities of the products and obtaining nanoscale molecular materials with both interesting magnetic properties and emissions in the visible part of the electromagnetic spectrum.

Acknowledgements

This work was supported by Brock University, NSERC-DG and ERA (to Th.C.S), the Alexander S. Onassis Public Benefit Foundation (graduate scholarship to P.S.P), the Fundação para a Ciência e a Tecnologia (FCT, Portugal) for financial support to REQUIMTE / LAQV (UID/QUI/50006/2013), and the DGICT (Project CTQ2015-63614-P, to A.E). V.B acknowledges financial support by the European Union (European Social Fund – ESF) and Greek national funds through the Operational Program "Education and Lifelong Learning" of the National Strategic Reference Framework (NSRF) - Research Funding Program: Archimedes III. The Advanced Light Source is supported by The Director, Office of Science, Office of Basic Energy Sciences of the U.S. Department of Energy, under contract no. DE-AC02-05CH11231.

Notes and references

1 For representative examples, see: a) A. J. Tasiopoulos, A. Vinslava, W. Wernsdorfer, K. A. Abboud and G. Christou, *Angew. Chem. Int. Ed.*, 2004, **43**, 2117-2121; b) G. F. S. Whitehead, F. Moro, G. A. Timco, W. Wernsdorfer, S. J. Teat and R. E. P. Winpenny, *Angew. Chem. Int. Ed.*, 2013, **125**, 10116-10119; c) R. T. W. Scott, S. Parsons, M. Murugesu, W. Wernsdorfer, G. Christou and E. K. Brechin, *Angew. Chem. Int. Ed.*, 2005, **44**, 6540-6543; d) M. Manoli, R. Inglis, M. J. Manos, V. Nastopoulos, W. Wernsdorfer, E. K. Brechin and A. J. Tasiopoulos, *Angew. Chem. Int. Ed.*, 2011, **50**, 4441-4444; e) M. Manoli, S. Alexandrou, L. Pham, G. Lorusso, W. Wernsdorfer, M. Evangelisti, G. Christou and A. J. Tasiopoulos, *Angew. Chem. Int. Ed.*, 2016, **55**, 679-684; f) P. Alborés and E. Rentschler, *Angew. Chem. Int. Ed.*, 2009, **48**, 9366-9370;

g) Z.- M. Zhang, S. Yao, Y.- G. Li, R. Clérac, Y. Lu, Z.- M. Su and E.- B. Wang, *J. Am. Chem. Soc.*, 2009, **131**, 14600-14601.

2 a) A. M. Ako, I. J. Hewitt, V. Mereacre, R. Clérac, W. Wernsdorfer, C. E. Anson and A. K. Powell, *Angew. Chem. Int. Ed.*, 2006, **45**, 4926-4929; b) C. J. Milios, A. Vinslava, W. Wernsdorfer, S. Moggach, S. Parsons, S. P. Perlepes, G. Christou and E. K. Brechin, *J. Am. Chem. Soc.*, 2007, **129**, 2754-2755; c) N. E. Chakov, S.- C. Lee, A. G. Harter, P. L. Kuhns, A. P. Reyes, S. O. Hill, N. S. Dalal, W. Wernsdorfer, K. Abboud and G. Christou, *J. Am. Chem. Soc.*, 2006, **128**, 6975-6989; d) R. J. Blagg, C. A. Muryn, E. J. L. McInnes, F. Tuna and R. E. P. Winpenny, *Angew. Chem. Int. Ed.*, 2011, **50**, 6530-6533; e) R. J. Blagg, L. Ungur, F.Tuna, J. Speak, P. Comar, D. Collison, W. Wernsdorfer, E. J. L. McInnes, L. Chibotaru and R. E. P. Winpenny, *Nature Chem.*, 2013, **5**, 673-678; f) J. D. Rinehart, M. Fang, W. J. Evans and J. R. Long, *Nature Chem.*, 2011, **3**, 538-542.

3 a) J.- C. G. Bünzli and S. V. Eliseeva, *Chem. Sci.*, 2013, 1939-1949; b) S. V. Eliseeva and J.- C. G. Bünzli, *New J. Chem.*, 2011, **35**, 1165-1176.

4 a) K. Griffiths, C. W. D. Gallop, A. Abdul-Sada, A. Vargas, O. Navarro and G. E. Kostakis, *Chem. Eur. J.*, 2015, **21**, 6358-6361; b) G. Maayan and G. Christou, *Inorg. Chem.*, 2011, **50**, 7015-7021; c) N. C. Anastasiadis, D. A. Kalofolias, A. Philippidis, S. Tzani, C. P. Raptopoulou, V. Psycharis, C. J. Milios, A. Escuer and S. P. Perlepes, *Dalton Trans.*, 2015, **44**, 10200-10209.

5 a) J. S. Kanady, E. Y. Tsui, M. W. Day and Th. Agapie, *Science*, 2011, **333**, 733-736; b) E. Y. Tsui, R. Tran, J. Yano and T. Agapie, *Nat. Chem.*, 2013, **5**, 293-299; c) S. Mukherjee, J. A. Stull, J. Yano, Th. C. Stamatatos, K. Pringouri, T. A. Stich, K. A. Abboud, R. D. Britt, V. K. Yachandra and G. Christou, *Proc. Natl. Acad. Sci. U. S. A.*, 2012, **109**, 2257-2262; d) C. Zhang, C. Chen, H. Dong, J.- R. Shen, H. Dau and J. Zhao, *Science*, 2015, **384**, 690-693.

6 a) E. K. Brechin, *Chem. Commun.*, 2005, 5141-5143; b) G. Aromí and E. K. Brechin, *Struct. Bond.*, 2006, **122**, 1-67; c) A. J. Tasiopoulos and S. P. Perlepes, *Dalton Trans.*, 2008, 5537-5555; d) Th. C. Stamatatos, C. G. Efthymiou, C. C. Stoumpos and S. P. Perlepes, *Eur. J. Inorg. Chem.*, 2009, 3361-3391.

7 a) C. J. Milios and R. E. P. Winpenny, *Struct. Bond.*, 2015, **164**, 1-109; b) R. E. P. Winpenny, *Adv. Inorg. Chem.*, 2001, **52**, 1-111; c) R. E. P Winpenny, *J. Chem. Soc., Dalton Trans.*, 2002, 1-10; d) A. A. Athanasopoulou, M. Pilkington, C. P. Raptopoulou, A. Escuer and Th. C. Stamatatos, *Chem. Commun.*, 2014, **50**, 14942-14945; e) Th. C. Stamatatos, K. A. Abboud, W. Wernsdorfer and G. Christou, *Angew. Chem. Int. Ed.*, 2008, **47**, 6694-6698.

8 a) C. Cadiou, M. Murrie, C. Pailsen, V. Villar, W. Wernsdorfer and R. E. P. Winpenny, *Chem. Commun.*, 2001, 2666-2667; b) E.- C. Yang, W. Wernsdorfer, L. N. Zakharov, Y. Karaki, A. Yamaguchi, R. M. Isidro, G.- D. Lu, S. A. Wilson, A. L. Rheingold, H. Ishimoto and D. Hendrickson, *Inorg. Chem.*, 2006, **45**, 529-546; c) M. Moragues-Canova, M. Helliwell, L. Ricard, E. Riviere, W. Wernsdorfer, E. K. Brechin and T. Mallah, *Eur. J. Inorg. Chem.*, 2004, 2219-2222; d) S. T. Ochsenbein, M. Murrie, E. Rusanov, H. Stoeckli-Evans, C. Sekine and H. U. Güdel, *Inorg. Chem.*, 2002, **41**, 5133-5140; e) G. Aromí, E. Bouwman, E. Burzurí, C. Carbonera, J. Krzystek, F. Luis, C. Schlegel, J. van Slageren, S. Tanase and S. J. Teat, *Chem. Eur. J.*, 2008, **14**, 11158-11166; f) G. Aromí, S. Parsons, W. Wernsdorfer, E. K. Brechin and E. J. L. McInnes, *Chem. Commun.*, 2005, 5038-5040.

9 a) J. K. McCusker, J. B. Vincent, E. A. Schmitt, M. L. Mino, K. Shin, D. K. Coggin, P. M. Hagen, J. C. Huffman, G. Christou and D. N. Hendrickson, *J. Am. Chem. Soc.*, 1991, **113**, 3012-3021; b) E. Libby, J. K. McCusker, E. A. Schmitt, K. Folting, D. N. Hendrickson and G. Christou, *Inorg. Chem.*, 1991, **31**, 3486-3495; c) O. Kahn, *Chem. Phys. Lett.*, 1997, **265**, 109-114.

10 a) O. Kahn, *Molecular Magnetism*; VCH Publishers: New York, 1993; b) C. Benelli and D. Gatteschi, *Chem. Rev.*, 2002, **102**, 2369-2388; c) R. Bagai and G. Christou, *Chem. Soc. Rev.*, 2009, **38**, 1011-1026.

11 a) L. Bogani and W. Wernsdorfer, *Nat. Mater.*, 2008, **7**, 179-186; b) R. Vincent, S. Klyatskaya, M. Ruben, W. Wernsdorfer and F. Balestro, *Nature*, 2012, **488**, 357-360; c) M. Urdampilleta, S. Klyatskaya, J.- P. Cleuziou, M. Ruben and W. Wernsdorfer, *Nat. Mater.*, 2011, **10**, 502-506.

12 a) A. Escuer, J. Esteban, S. P. Perlepes and Th. C. Stamatatos, *Coord. Chem. Rev.*, 2014, **275**, 87-129; b) Th. C. Stamatatos and G. Christou, *Inorg. Chem.*, 2009, **48**, 3308-3322; c) M. Andruh, *Dalton Trans.*, 2015, **44**, 16633-16653; d) M. Murrie, *Chem. Soc. Rev.*, 2010, **39**, 1986-1995.

13 a) J.- M. Lehn, *Angew. Chem. Int. Ed.*, 1990, **29**, 1304-1319; b) K. Binnemans, *Chem. Rev.*, 2009, **109**, 4283-4374; c) Y. Y. Chia and M. G. Tay, *Dalton Trans.*, 2014, **43**, 13159-13168; d) P. D. Fleischauer and P. Fleischauer, *Chem. Rev.*, 1970, **70**, 199-230.

14 P. S. Perlepe, L. Cunha-Silva, K. J. Gagnon, S. J. Teat, C. Lampropoulos, A. Escuer and Th. C. Stamatatos, *Inorg. Chem.*, 2016, **55**, 1270-1277.

15 T. Kottke and D. Stalke, *J. App. Cryst.*, 1993, **26**, 615.

16 APEX2, Data Collection Software Version 2012.4, Bruker AXS, Delft, The Netherlands, 2012.

17 Cryopad, Remote monitoring and control, Version 1.451, Oxford Cryosystems, Oxford, United Kingdom, 2006.

18 SAINT+, *Data Integration Engine v. 8.27b*©, 1997-2012, Bruker AXS, Madison, Wisconsin, USA.

19 G. M. Sheldrick, SADABS 2012/1, Bruker AXS Area Detector Scaling and Absorption Correction Program, 2012, Bruker AXS, Madison, Wisconsin, USA.

20 G. M. Sheldrick, *Acta Cryst. A*, 2008, **64**, 112.

21 G. M. Sheldrick, SHELXT v. 2014/3, Program for Crystal Structure Solution, University of Göttingen, 2014.

22 G. M. Sheldrick, SHELXL v. 2014, Program for Crystal Structure Refinement, University of Göttingen, 2014.

23 P. Van der Sluis and A. L. Spek, *Acta Cryst. A*, 1990, **46**, 194.

24 a) A. L. Spek, *Acta Cryst. A*, 1990, **46**, C34; b) A. L. Spek, *J. Appl. Crystallogr.*, 2003, **36**, 7.

25 G. A. Bain and J. F. Berry, *J. Chem. Educ.*, 2008, **85**, 532-536.

26 N. F. Chilton, R. P. Anderson, L. D. Turner, A. Soncini and K. S. Murray, *J. Comput. Chem.*, 2013, **34**, 1164-1175.

27 For some representative heterometallic 3d-Na and 3d-K clusters, see: a) Th. C. Stamatatos, A. Escuer, K. A. Abboud, C. P. Raptopoulou, S. P. Perlepes and G. Christou, *Inorg. Chem.*, 2008, **47**, 11825-11838; b) D. I. Alexandropoulos, E. C. Mazarakioti, S. J. Teat and Th. C. Stamatatos, *Polyhedron*, 2013, **64**, 91-98; c) G. Aromí, A. R. Bell, M. Helliwell, J. Raftery, S. J. Teat, G. A. Timco, O. Roubeau and R. E. P. Winpenny, *Chem. Eur. J.*, 2003, **9**, 3024-3031; d) M. Murugesu, R. Clérac, C. E. Anson and A. K. Powell, *Chem. Commun.*, 2004, 1598-1599.

28 a) P. S. Perlepe, A. A. Athanasopoulou, K. I. Alexopoulou, C. P. Raptopoulou, V. Psycharis, A. Escuer, S. P. Perlepes and Th. C. Stamatatos, *Dalton. Trans.*, 2014, **43**, 16605-16609; b) A. A. Athanasopoulou, C. P. Raptopoulou, A. Escuer and Th. C. Stamatatos, *RSC Adv.*, 2014, **4**, 12680-12684.

29 a) C. Papatriantafyllopoulou, G. Aromí, A. J. Tasiopoulos, V. Nastopoulos, C. P. Raptopoulou, S. J. Teat, A. Escuer and S. P. Perlepes, *Eur. J. Inorg. Chem.*, 2007, 2761; b) P. Chaudhuri, T. Weyhermüller, R. Wagner, S. Khanra, B. Biswas, E. Bothe and E. Bill, *Inorg. Chem.*, 2007, **46**, 9003; c) A. Escuer, J. Esteban, N. Aliaga-Alcalde, M. Font-Bardia,

T. Calvet, O. Roubeau and S. J. Teat, *Inorg. Chem.*, 2010, **49**, 2259; d) S. Zhang, L. Zhen, B. Xu, R. Inglis, K. Li, W. Chen, Y. Zhang, K. F. Konidaris, S. P. Perlepes, E. K. Brechin and Y. Li, *Dalton Trans.*, 2010, **39**, 3563; e) K. I. Alexopoulou, A. Terzis, C. P. Raptopoulou, V. Psycharis, A. Escuer and S. P. Perlepes, *Inorg. Chem.*, 2015, **54**, 5615-5617.

30 a) S. Das, L. Sorace, A. Guha, R. Sanyal, H. Kara, A. Caneschi, E. Zangrando and D. Das, *Eur. J. Inorg. Chem.*, 2014, 2753-2765; b) J. Esteban, M. Font-Bardia and A. Escuer, *Inorg. Chem.*, 2014, **53**, 1113-1121; c) H. Adams, S. Clunas, D. E. Fenton and D. N. Towers, *J. Chem. Soc., Dalton Trans.*, 2002, 3933-3935; d) A. J. Finney, M. A. Hitchman, C. L. Raston, G. L. Rowbottom and A. H. White, *Aust. J. Chem.*, 1981, **34**, 2139-2157; e) G. N. Newton, H. Sato, T. Shiga and H. Oshio, *Dalton Trans.*, 2013, **42**, 6701-6704; f) T. K. Paine, E. Rentschler, T. Weyhermuller and P. Chaudhuri, *Eur. J. Inorg. Chem.*, 2003, 3167-3178; g) W. L. Leong and J. J. Vittal, *New J. Chem.*, 2010, **34**, 2145-2152; h) A. Guha, A. Banerjee, R. Mondol, E. Zangrando and D. Das, *J. Coord. Chem.*, 2011, **64**, 3872-3886; i) Y. Wei, H. Hou, Y. Fan and Y. Zhu, *Eur. J. Inorg. Chem.*, 2004, 3946-3957; j) J. Esteban, E. Ruiz, M. Font-Bardia, T. Calvet and A. Escuer, *Chem. Eur. J.*, 2012, **18**, 3637-3648; k) A. K. Ghosh, M. Shatruk, V. Bertolasi, K. Pramanik and D. Ray, *Inorg. Chem.*, 2013, **52**, 13894-13903; l) T. Peristeraki, M. Samios, M. Siczek, T. Lis and C. J. Milios, *Inorg. Chem.*, 2011, **50**, 5175-5185.

31 a) Y.- W. Tzeng, C.- J. Lin, M. Nakano, C.- I. Yang, W.- L. Wan and L.- L. Lai, *Dalton Trans.*, 2014, **43**, 3044-3047; b) A. Scheurer, K. Gieb, M. S. Alam, F. W. Heinemann, R. W. Saalfrank, W. Kroener, K. Petukhov, M. Stocker and P. Müller, *Dalton Trans.*, 2012, **41**, 3553-3561; c) M. Fondo, N. Ocampo, A. M. García-Deibe, J. Cano and J. Sanmartín, *Dalton Trans.*, 2010, **39**, 10888-10899; d) A. D. Katsenis, V. G. Kessler and G. S. Papaefstathiou, *Dalton Trans.*, 2011, **40**, 4590-4598; e) C. Cadiou, R. A. Coxall, A. Graham, A. Harrison, M. Helliwell, S. Parsons and R. E. P. Winpenny, *Chem. Commun.*, 2002, 1106-1107.

32 S. Wörl, H. Pritzkow, I. O. Fritsky and R. Krämer, *Dalton Trans.*, 2005, 27-29.

33 A. W. Addison, T. N. Rao, J. Reedijk, J. Rijn and G. C. Verschoor, *J. Chem. Soc., Dalton Trans.*, 1984, 1349-1356.

34 a) Th. C. Stamatatos, E. Diamantopoulou, A. Tasiopoulos, V. Psycharis, R. Vicente, C. P. Raptopoulou, V. Nastopoulos, A. Escuer and S. P. Perlepes, *Inorg. Chim. Acta*, 2006, **359**, 4149-4157; b) S. Khanra, T. Weyhermüller, E. Rentschler and P. Chaudhuri, *Inorg. Chem.*, 2005, **44**, 8176-8178; c) S. K. Langley, M. Helliwell, S. J. Teat and R. E. P. Winpenny, *Inorg. Chem.*, 2014, **53**, 1128-1134; d) B. Biswas, U. Pieper, T. Weyhermüller and P. Chaudhuri, *Inorg. Chem.*, 2009, **48**, 6781-6793.

35 W. Liu and H. H. Thorp, *Inorg. Chem.*, 1993, **32,** 4102-4105.

36 a) M. A. Palacios, A. J. Mota, J. E. Perea-Buceta, F. J. White, E. K. Brechin and E. Colacio, *Inorg. Chem.*, 2010, **49**, 10156–10165; b) A. Greatti, M. Scarpellini, R. A. Peralta, A. Casellato, A. J. Bortoluzzi, F. R. Xavier, R. Jovito, M. Aires de Brito, B. Szpoganicz, Z. Tomkowicz, M. Rams, W. Haase and A. Neves, *Inorg. Chem.*, 2008, **47**, 1107-1119; c) M. S. El Fallah, F. Badyine, R. Vicente, A. Escuer, X. Solans and M. Font-Bardia, *Dalton Trans.*, 2006, 2934-2942, and references cited therein.

37 a) M. Murugesu, R. Clérac, B. Pilawa, A. Mandel, C. E. Anson and A. K. Powell, *Inorg. Chim. Acta*, 2002, **337**, 328-336; b) E. Colacio, J. M. Domínguez-Vera, M. Ghazi, R. Kivekäs, M. Klinga and J. M. Moreno, *Eur. J. Inorg. Chem.*, 1999, 441-445.

38 a) J.- C. G. Bünzli and C. Piguet, *Chem. Soc. Rev.*, 2005, **34**, 1048-1077; b) M. Barwiolek, *E.* Szlyk, T. M. Muziol and T. Lis, *Dalton Trans.*, 2011, **40**, 11012-11022; c) A. Alaimo, D. Takahashi, L. Cunha-Silva, G. Christou and Th. C. Stamatatos, *Inorg. Chem.*, 2015, **54**, 2137−2151; d) D. I. Alexandropoulos, A. M. Mowson, M. Pilkington, V. Bekiari and G. Christou, *Dalton Trans.*, 2014, **43**, 1965-1969.